Facultad de Ciencias

Sección de Física

---

# *Numerical simulations of micro and nano-structured optical waveguides inside YAG crystals*

---


Author: **Paul Santos Ramos**

Supervised by: **Omar de Varona Ortega**

With assistance of: **Airán Ródenas Seguí**

# Contents

# 1 Abstract

The formation and propagation of light waves inside an Er:YAG photonic crystal has been studied for a pattern of concentric rings formed by air pores; with the purpose of applying it in optical systems incorporating conventional optical fibres, using simulations performed by means of the *RSoft CAD:BeamPROP* and *WinPLOT* softwares. Firstly, the importance of obtaining new laser sources in eye-safe wavelength regions in the current scientific and technological context is highlighted, and how the implementation of these structures would be a breakthrough for generating and propagating this type of waves. Secondly, a brief introduction is given to the functioning of laser devices, optical fibres and the theoretical basis of the study of photonic crystals. The properties of this new type of photonic crystal structure and its manufacturing method are also discussed. Once the theoretical part has been explained, the operation of the *RSoft CAD:BeamPROP* program, which allows photonic crystals to be modelled with the desired conditions, and the *WinPLOT* data analysis program are presented and explained. In the first part, simulations were conducted to analyze the emission of a wave with a wavelength of 1645 nm from an Er:YAG crystal towards an optical fiber. The focus was on investigating the fundamental modes of different configurations of a structure composed of concentric rings of pores and examining the parameters that affect the distribution of the electric field within the mode. In the second part, simulations were performed to study the propagation of the previously obtained fundamental modes. The objective was to analyze and identify the factors within the structure of the concentric ring pores that impact the power transmitted by the wave through the material. The factors contributing to the formation and propagation of higher-order modes were also examined to determine the optimal configuration that minimizes losses during propagation and the formation of higher-order modes. Finally, the reverse scenario was explored in which a conventional optical fiber, referred to as '6/125 Precision Matched Passive Single-Mode 1550-nm Double Clad Fiber', with a mode field diameter (MFD) of 7.4 $\mu$m, directs a Gaussian wave with a wavelength corresponding to one of the emission wavelengths of Er:YAG crystal, specifically $\lambda = 1645$ nm, towards the crystal. Similar to the previous section, the analysis focused on identifying the factors within the structure of the concentric ring pores that influence the power transmitted by the wave through the material, losses due to wave coupling, and the generation of higher-order modes during propagation.

# 2 Resumen

Se ha estudiado la formación y propagación de ondas de luz dentro de un cristal fotónico Er:YAG para un patrón de anillos concéntricos formados por poros de aire nunca antes estudiado; con el propósito de aplicarlo en sistemas ópticos que incorporen fibras ópticas convencionales, utilizando simulaciones realizadas mediante los softwares *RSoft CAD:BeamPROP* y *WinPLOT*. En primer lugar, se destaca la importancia de obtener nuevas fuentes de láseres en regiones de longitudes de onda seguras para los ojos, en el contexto científico y tecnológico actual, y cómo la implementación de estas estructuras sería un gran avance para generar y propagar este tipo de ondas. En segundo lugar, se realiza una breve introducción al funcionamiento de los dispositivos láser, a las fibras ópticas y a las bases teóricas del estudio de los cristales fotónicos. También se discuten las propiedades que presenta este nuevo tipo de estructura de cristal fotónico y cuál es su método de fabricación. Una vez explicada la parte teórica, se expone y se explica el funcionamiento del programa *RSoft CAD:BeamPROP*, que permite modelar cristales fotónicos con las condiciones deseadas, y del programa de análisis de datos *WinPLOT*. En la primera parte, se realizaron simulaciones para analizar la emisión de una onda con una longitud de onda de 1645 nm desde un cristal de Er:YAG hacia una fibra óptica. El enfoque se centró en investigar los modos fundamentales de diferentes configuraciones de una estructura compuesta por anillos concéntricos de poros y examinar los parámetros que afectan la distribución del campo eléctrico dentro del modo. En la

segunda parte, se llevaron a cabo simulaciones para estudiar la propagación de los modos fundamentales obtenidos anteriormente. El objetivo fue analizar e identificar los factores dentro de la estructura de los poros en forma de anillos concéntricos que impactan la potencia transmitida por la onda a través del material. También se examinaron los factores que contribuyen a la formación y propagación de los modos de orden superior, con el fin de determinar la configuración óptima que minimiza las pérdidas durante la propagación y la formación de los modos de orden superior. Por último, se exploró el escenario inverso en el cual una fibra óptica convencional, denominada '6/125 Precision Matched Passive Single-Mode 1550-nm Double Clad Fiber', con un diámetro del campo del modo (MFD) de 7.4 $\mu$m, dirige una onda gaussiana con una longitud de onda correspondiente a una de las longitudes de emisión del cristal de Er:YAG, específicamente $\lambda = 1645$ nm, hacia el cristal. Al igual que en la sección anterior, el análisis se centró en identificar los factores dentro de la estructura de los poros en forma de anillos concéntricos que influyen en la potencia transmitida por la onda a través del material, las pérdidas debidas al acople de la onda y la generación de modos de orden superior durante la propagación.

# 3 Objectives

The objectives of this work are as follows:

1. Design and numerically simulate micro-nanostructured optical waveguides inside YAG optical crystals for the near-infrared range.
2. Utilize simulation tools for photonics systems based on finite element methods (FEM) and finite-difference time-domain (FDTD) techniques.
3. Pave the way in the research and development of systems that combine conventional optical fibers with photonic crystals.
4. Contribute to the research lines of the research group and address the real needs of European and national research projects.

# 4 Objetivos

Los objetivos de este trabajo son los siguientes:

1. Diseñar y simular numéricamente guías de ondas ópticas micro-nanoestructuradas dentro de cristales ópticos de YAG para el rango del infrarrojo cercano.
2. Utilizar herramientas de simulación para sistemas fotónicos basadas en métodos de elementos finitos (FEM) y técnicas de diferencia finita en el dominio del tiempo (FDTD).
3. Abrir el camino en la investigación y desarrollo de sistemas que combinen fibras ópticas convencionales con cristales fotónicos.
4. Contribuir a las líneas de investigación del grupo de investigación y abordar las necesidades reales de proyectos de investigación europeos y nacionales.

# 5 Introduction

En los últimos años, las fuentes láser que operan en una longitud de onda segura para los ojos han adquirido gran importancia debido a sus diversas aplicaciones, como el sensado remoto y la comunicación en espacio libre. Por esta razón, el desarrollo de sistemas ópticos que permitan la formación y propagación sin pérdidas de estos láseres se ha vuelto crucial. Los recientes avances en cristales fotónicos y las revoluciones tecnológicas en física aplicada, como la fotónica, han demostrado ser herramientas poderosas para lograr este objetivo. En este estudio, se analizó un sistema compuesto por una fibra óptica y un cristal fotónico de Er:YAG con un patrón no estudiado previamente hasta donde se pudo comprobar. El cristal fotónico consiste en anillos concéntricos formados por poros circulares de aire, que facilitan la propagación de la luz y filtran los modos superiores. En la primera parte, se realizaron simulaciones para analizar la emisión de una onda con una longitud de onda de 1645 nm desde un cristal de Er:YAG hacia una fibra óptica. El enfoque se centró en investigar los modos fundamentales de diferentes configuraciones de una estructura compuesta por anillos concéntricos de poros y examinar los parámetros que afectan la distribución del campo eléctrico dentro del modo. Pasando a la segunda parte, se realizaron simulaciones para estudiar la propagación de los modos fundamentales obtenidos en la sección anterior. El objetivo era analizar e identificar los factores dentro de la estructura de los poros en forma de anillos concéntricos que afectan a la potencia transmitida por la onda a través del material. Además, se examinaron los factores que contribuyen a la formación y propagación de los modos de orden superior para determinar la configuración óptima que minimiza las pérdidas durante la propagación y la formación de los modos de orden superior. Por último, se exploró el escenario inverso en el cual la fibra óptica emite una onda gaussiana con una longitud de onda correspondiente a una de las longitudes de onda de emisión del cristal de Er:YAG, específicamente $\lambda$=1645 nm. Al igual que en la sección anterior, el análisis se centró en identificar los factores dentro de la estructura de los poros en forma de anillos concéntricos que influyen en la potencia transmitida por la onda a través del material, las pérdidas debidas al acople de la onda y la generación de modos de orden superior durante la propagación.

Lasers operating in the eye-safe wavelength region, around $1.5 - 1.6\mu$m, have various applications such as remote sensing, distance measurement, and free-space communications [ref:1]. Direct pumping of Er:YAG using an Er,Yb fiber laser has emerged as one of the primary choices to achieve this wavelength, due to its ability to generate high average output power in both continuous-wave and Q-switched modes. Consequently, the development of optical systems enabling lossless formation and propagation of these lasers has gained significant importance.

Recent discoveries in the formation and study of photonic crystals have become important in this context. The manipulation of the optical properties of materials through the development of band theory and the discovery of energy gaps has led to advancements in applied physics, specifically in the field of photonics, which aims to control photons in a similar manner as electrons. Implementing photonic crystals in systems composed of conventional fibers opens up new perspectives in the field of optics, enabling the creation of optical systems capable of generating and propagating light coherently and efficiently, with high spectral selectivity and minimal interference.

In this work, we have analyzed a system consisting of an optical fiber "6/125 Precision Matched Passive Single-Mode 1550-nm Double Clad Fiber" [ref:2]with a mode field diameter (MFD) of 7.4 $\mu$m, coupled to an Er:YAG photonic crystal with a previously unstudied pattern, as far as could be verified. The photonic crystal is composed of concentric rings formed by circular air pores,

which facilitate the propagation of light while filtering out higher-order modes. We divided our study into three parts:

In the first part, we performed simulations of the emission of a wave with a wavelength of 1645 nm from an Er:YAG crystal towards an optical fiber. We investigated the fundamental modes of various configurations of a structure consisting of concentric rings of pores and examined the parameters that impact the electric field distribution within the mode.

In the second part, we simulated the propagation of the fundamental modes obtained in the previous section to analyze and identify the factors within the structure of concentric ring pores that affect the power transmitted by the wave through the material. We also examined the factors that contribute to the formation and propagation of higher order modes with the aim of determining the optimal configuration that minimizes losses during propagation and the formation of higher order modes.

In the final part, we investigated the reverse scenario where an optical fiber emits a gaussian wave with a wavelength that matches one of the emission wavelengths of the Er:YAG crystal, specifically $\lambda$=1645 nm. Following a similar approach as in the previous section, our analysis focused on identifying the factors within the structure of concentric ring pores that affect the power transmitted by the wave through the material, the losses due to wave coupling, and the generation of higher-order modes during propagation.

By employing this computational approach, our aim was to gain a comprehensive understanding of this new type of photonic crystal structures and their specific applications. This research provides valuable insights into the design and optimization of photonic structures for efficient light manipulation and control, ultimately advancing the field of photonics. The findings of this study have implications for various photonics applications, including optical communication, sensing, and integrated photonics devices, leading to enhanced functionality and performance.

# 6 Methodology

En esta sección se presenta una breve introducción a los dispositivos láser, explicando el proceso mediante el cual un cristal de Er:YAG emite ondas de luz a una longitud de onda de $\lambda$ = 1645 nm. También se aborda el funcionamiento de las fibras ópticas, junto con la introducción del concepto de Diámetro del Campo del Modo (MFD) y su relevancia en las fibras monomodo. Además, se introduce la teoría de los cristales fotónicos, que son materiales con una función dieléctrica periódica. Se presenta un nuevo tipo de estructura de cristal fotónico formada por anillos concéntricos de poros, que tiene la capacidad de filtrar modos superiores al fundamental debido a su mayor propensión a las pérdidas de energía en modos no fundamentales durante la propagación. También se describe el proceso de fabricación de estas estructuras mediante fotomodificación inducida por láser. Posteriormente, se procede a explicar los tipos de pérdidas de potencia que se presentan en el sistema que queremos analizar. A continuación, se introduce el software *RSoft CAD:BeamPROP* y *WinPLOT*, explicando cómo se calcula la propagación de las ondas en las simulaciones y cómo se configuran en cada programa. Por último, se detalla el procedimiento llevado a cabo en cada simulación y la obtención de los datos correspondientes.

## 6.1 Erbium:YAG Crystal as an Active Medium for Coherent Light Generation

Lasers are devices that generate coherent light through a process of amplification of stimulated radiation. Basically, lasers consist of an active medium (such as a crystal, gas or semiconductor) sandwiched between two mirrors. The active medium is excited by some external means (such as optical or electrical pumping) and, when the atoms in the active medium emit photons, these photons are reflected by the mirrors, amplifying the light and producing a coherent beam of light.

In our case, the active medium is an Erbium:YAG crystal. This crystal is a type of optical crystal that is doped with erbium ions (Er3+) and has a composition mainly of yttrium-aluminium-garnet (YAG). The crystal is doped with erbium ions to obtain specific optical properties.

The erbium ions ($Er^{3+}$) in the Er:YAG crystal are incorporated into the crystal structure. Erbium is a trivalent ion, which means that it has lost three electrons and has acquired a positive charge of +3. These erbium ions occupy specific positions in the YAG crystal lattice, replacing some of the yttrium (Y) ions in the structure.

When the Er:YAG crystal is excited by energy absorption, the erbium ions can undergo transitions between different energy levels. Specifically, in the transition $4I_{13/2} \rightarrow 4I_{15/2}$ [ref:3] [ref:4] at a wavelength of 1645 nm, these transitions occur. These transitions generate coherent light emission, which allows the laser to operate at the desired wavelength.

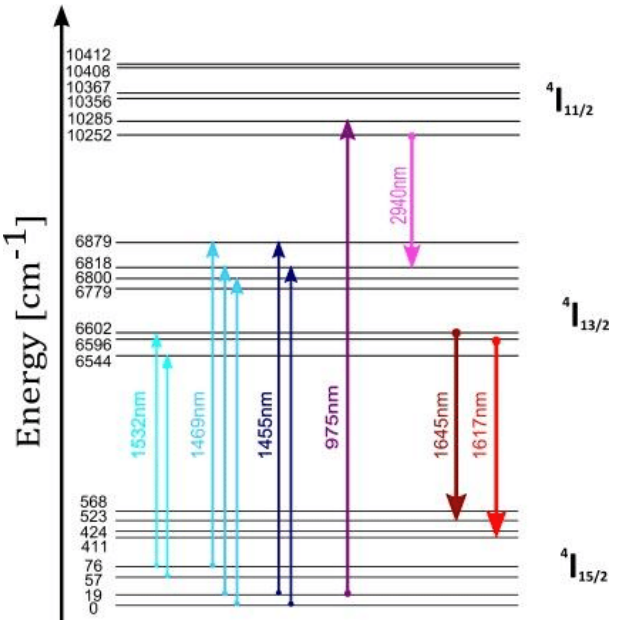


Figure 1: Diagram of energy levels of the Er:YAG crystal

## 6.2 Introduction to Optical Fibers

Optical fibres are a fundamental component of modern communications and data transmission systems. These fibres, made of highly transparent dielectric material, allow information to be transmitted as pulses of light over long distances.

The most common optical fibres are known as total internal reflection fibers, which allow wave propagation by means of the principle of total internal reflection. In the core of the fibre, which is made of a material with a higher refractive index than the surrounding cladding, light propagates through multiple internal reflections.

In optical systems, the interconnection of multiple optical fibers in a series is often required, leading to potential losses at the splice points. In the case of multimode fibers, compatibility is achieved by ensuring similarity in core diameters, which aids in minimizing losses. However, for single-mode fibers, this criterion alone does not ensure compatibility.

To elucidate this, it is crucial to comprehend that a portion of the propagating wave in an optical fiber travels through the cladding. While this phenomenon is negligible in multimode fibers and typically disregarded, it assumes significance in single-mode fibers. This is where the Mode Field Diameter (MFD) [ref:5] [ref:6] becomes relevant. Being a fundamental parameter in optical fibers, the MFD is defined as the diameter at which the wave's intensity has diminished to a value proportional to $1/e^2$ or equivalently, the distance from the center at which the electric and magnetic field strengths are reduced to $1/e$ of their maximum values. Unlike the core size, the MFD is an optical value that can vary with the wavelength employed.

In general, the greater the difference in MFD, the greater the attenuation experienced at the splice. Therefore, it is essential to consider the MFD when designing and working with optical systems involving single-mode fibres in order to ensure proper compatibility and minimise splice losses.

In addition to MFD, another important parameter in single-mode fibers is the V-factor [ref:7].

The V-factor provides us with additional information about the possible modes within an optical fiber. In the specific case of an optical fiber, the effective V-factor ($V$) is defined using the formula:

$$V = \frac{2 \cdot \pi}{\lambda} \cdot a \cdot NA = \frac{2 \cdot \pi}{\lambda} \cdot a \cdot \sqrt{n_{core}^2 - n_{cladding}^2} \tag{1}$$

Here, $\lambda$ represents the vacuum wavelength, $a$ is the radius of the fiber core, $NA$ denotes the numerical aperture, and $n_{core}$ and $n_{cladding}$ are the refractive indices of the core and cladding, respectively.

For values below approximately 2.405, the fiber supports only one mode per polarization direction, resulting in single-mode fibers. On the other hand, multimode fibers can support a larger number of modes. The number of supported modes in a step-index fiber, including polarization multiplicity, can be approximately calculated based on the V-factor.

The V-factor also determines the fraction of optical power in a specific mode that is confined to the fiber core. For single-mode fibers, this fraction is low for low V-factor values, but it reaches approximately 90% near the single-mode cut-off at V $\approx$ 2.405.

## 6.3 Introduction to Fundamental Concepts and Optical Properties of Photonic Crystals

A photonic crystal is a solid structure that uses a periodic dielectric function to control and manipulate the propagation of light[ref:8]. Similar to how electrons propagate in conducting crystals, photonic crystals can selectively block certain wavelengths of light and allow others to propagate. We can apply similar concepts to those used in conducting crystals to understand how photonic crystals work, such as lattice vectors, which define the position of each point in the lattice, and the unit cell, which is a portion of the lattice that can be repeated to form the complete structure.

Macroscopic electromagnetism, including the propagation of light in a photonic crystal, is governed by Maxwell's equations. To understand how these crystals work, we will focus on lossless, transparent, non-dispersive, linear materials where there are no free charges or currents.

$$\nabla \cdot \mathbf{H}(\mathbf{r}, t) = 0 \tag{2}$$

$$\nabla \cdot (\epsilon(\mathbf{r}) \cdot \mathbf{E}(\mathbf{r}, t)) = 0 \tag{3}$$

$$\nabla \times \mathbf{E}(\mathbf{r}, t) + \mu_0 \cdot \frac{\partial \mathbf{H}(\mathbf{r}, t)}{\partial t} = 0 \tag{4}$$

$$\nabla \times \mathbf{H}(\mathbf{r}, t) - \epsilon_0 \cdot \epsilon(\mathbf{r}) \cdot \frac{\partial \mathbf{E}(\mathbf{r}, t)}{\partial t} = 0 \tag{5}$$

The position vector $\mathbf{r}$ represents the three-dimensional spatial coordinates, while $\epsilon_0$ denotes the vacuum permittivity, and $\mu_0$ represents the vacuum permeability, which are fundamental constants. The electric and magnetic fields, $\mathbf{E}(\mathbf{r}, t)$ and $\mathbf{H}(\mathbf{r}, t)$ respectively, are vectors that depend on both position $\mathbf{r}$ and time $t$.

In these materials, the dielectric function $\epsilon(\mathbf{r})$ is a real number. Maxwell's equations are linear, which allows us to separate the spatial and temporal dependence of the $\mathbf{E}$ and $\mathbf{H}$ fields by composing them as a series of harmonic modes.

In this way, we can rewrite each field as follow:

$$\mathbf{H}(\mathbf{r}, t) = \mathbf{H}(\mathbf{r}) \cdot \mathrm{e}^{-i \cdot w \cdot t} \tag{6}$$

$$\mathbf{E}(\mathbf{r}, t) = \mathbf{E}(\mathbf{r}) \cdot \mathrm{e}^{-i \cdot w \cdot t} \tag{7}$$

If we substitute these equations into Maxwell's Equations 4 and 5, we would have:

$$\nabla \times \mathbf{E}(\mathbf{r}) - i \cdot w \cdot \mu_0 \cdot \mathbf{H}(\mathbf{r}) = 0 \tag{8}$$

$$\nabla \times \mathbf{H}(\mathbf{r}) + i \cdot w \cdot \epsilon_0 \cdot \epsilon(\mathbf{r}) \cdot \mathbf{E}(\mathbf{r}) = 0 \tag{9}$$

We can decouple the equations as follows. We divide the last equation by $\epsilon(\vec{r})$ and apply the rotational operator. Then we use the first equation to eliminate $\mathbf{E}(\mathbf{r})$. Furthermore, the constants $\epsilon_0$ and $\mu_0$ satisfy $c = 1/\sqrt{\epsilon_0 \cdot \mu_0}$, where $c$ is the vacuum speed of light. Resulting in an operation dependent only on $\mathbf{H}(\mathbf{r})$:

$$\nabla \times \left( \frac{1}{\epsilon(\mathbf{r})} \cdot \nabla \times \mathbf{H}(\mathbf{r}) \right) = \left( \frac{w}{c} \right)^2 \cdot \mathbf{H}(\mathbf{r}) \tag{10}$$

This equation, referred to as the "master equation", tells us everything we need to know about $\mathbf{H}(\mathbf{r})$. The same formula could also have been obtained as a function of $\mathbf{E}(\mathbf{r})$.

The Equation 10 is the heart of Maxwell's equations for a harmonic mode in a mixed dielectric medium. This equation is an eigenvalue problem for the operator $\Theta = \nabla \times (\frac{1}{\epsilon(\mathbf{r})} \cdot \nabla \times)$, which must be hermetic, since otherwise it would be possible to obtain complex $w$ frequencies, which does not make physical sense. Moreover, being a hermitic operator, it is fulfilled that its eigenfunctions corresponding to different eigenvalues are orthogonal. That is to say, if we define the scalar product of two fields as:

$$(\mathbf{F}, \mathbf{G}) = \int \mathbf{F^*}(\mathbf{r}) \cdot \mathbf{G}(\mathbf{r}) \cdot d^3 r \tag{11}$$

And if we define two eigenfunctions $\mathbf{H_1}$ and $\mathbf{H_2}$ with eigenvalues $w_1$ and $w_2$ respectively, satisfying that $w_1 \neq w_2$; we have that $(\mathbf{H_1}, \mathbf{H_2}) = (\mathbf{H_2}, \mathbf{H_1}) = 0$.

So far we have dealt with generic inhomogeneous media, but in this work we focus on photonic crystals, which requires imposing the periodicity condition: such a system does not change if everything is translated over the same distance in a given direction. In fact, a system that exhibits translational symmetry in all three spatial directions is a homogeneous medium, whose modes fulfil a similar relation described in Bloch's Theorem:

$$\mathbf{H}_k(\mathbf{r}) = e^{i \cdot \mathbf{k} \cdot \mathbf{r}} \cdot \mathbf{u}_k(\mathbf{r}) \tag{12}$$

As with electrons in solids, the frequency of each mode will be determined by the direction of propagation in the lattice, resulting in the formation of the frequency bands. The smallest unit capable of generating the complete band structure by repetition is known as a unit cell in reciprocal space or simply a Brillouin zone. Occasionally, it may happen that in no direction is it possible to find a finite range of frequencies, which gives rise to the well-known photonic band gaps. These band gaps are one of the reasons why photonic crystals are so interesting.

Having explained the fundamental concepts of photonic crystals, we can now move on to explain the type of photonic crystal structures that will be the focus of this paper.

### 6.3.1 Structure of concentric rings formed by pores

The objective of this research is to examine a particular configuration characterized by the presence of concentric rings composed of circular air pores. This structure possesses an intriguing characteristic: the modes traversing the structure experience attenuation due to energy leakage between

the pores in each ring. Notably, the non-fundamental modes are more susceptible to this effect, as their field distribution facilitates such losses. This property holds significant value in numerous investigations as it enables the elimination of undesired modes within the crystal, allowing only the desired mode to be obtained at the end of the process.

The degree of attenuation encountered by the wave passing through this structure varies based on several parameters, including the refractive index of the crystal and pores, the diameter of the rings, the number and spacing of the pores, as well as the shape and width of the pores, among others.

Although this type of structure lacks the periodicity observed in traditional photonic crystals in the Cartesian plane, it does exhibit radial periodicity measured from the central point of the structure, which has not been explored previously. Therefore, it is plausible to consider these structures as a novel type of photonic crystal.

The lack of Cartesian periodicity in structures of this nature presents a significant hurdle for their analytical investigation. Consequently, computational simulations serve as a valuable initial approach to studying such structures.

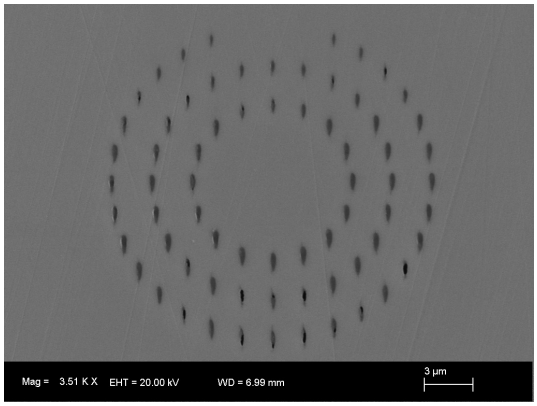


Figure 2: Picture of a three-ring structure.

### 6.4 Manufacturing and Formation Process for Porous Structures in Crystals

The formation of these structures involves an innovative process for creating air pores that utilizes the three-dimensional laser writing (3DLW) technique [ref:9] [ref:10]. Initially, straight lines with submicrometer width are created in an XY plane within the YAG crystal. Subsequently, a polishing process is performed on the lithographed area until reaching one end of the lines, thereby establishing the porous structure for the subsequent step.

To understand how this method is carried out, its process will be divided into three distinct steps for explanation:

1. Preparation of the porous structure: In the photomodification process of the YAG crystal. A specific laser frequency is carefully selected to render the crystal transparent, effectively inhibiting electronic transitions within that frequency range. However, the chosen frequency remains sufficiently high to induce transitions from the ground state to intermediate virtual

states.

By focusing the laser intensity at or near the focal point, a region of high energy density is achieved. This leads to multiphoton absorption, a nonlinear process that modifies the chemical bonds in the crystal without breaking them. These modifications result in alterations of the internal structure, as well as the physical and chemical properties of the crystal, including its susceptibility to chemical attack.

2. Exposure of photomodified tracks: An intermediate step between 3DLW and wet-chemical etching is required if the written nanotracks are all inside the crystal far from its superficial faces. To initiate the wet-etching reaction, either polishing of the sample is performed to expose laser-written tracks to the sample surface or vertically written tracks, which start from the surface to the written lattice, are included. This allows wet-etching of the 3DLW structure directly without lateral polishing. Optical polishing is a mechanical process that can be done easily and only requires that some tracks are written closer to the sample facets, so that polishing is a fast and simple process leading to an optical quality surface. Polishing the sample until the written tracks are exposed to air has the advantage of facilitating the study of the cross-section morphologies of the written structures by SEM. In the case of writing vertical pores to serve as inlets for the acid instead, these extra pores serve to selectively etch a larger volume of written structures within the crystal and can also be utilized to further engineer the device architectures with local 3D control inside the sample.

3. Wet-chemical etching: Wet-chemical etching of 3DLW structures within YAG crystals involves immersing the samples in a specific solution, such as a 44 w.t.% phosphoric acid (H3PO4) solution in deionized water, at a controlled temperature of 350 K. During the etching process, a chemical reaction occurs between the YAG crystal and the phosphoric acid solution, described by the equation: $Y_3Al_5O_{12} + 8H_3PO_4 \rightarrow 3YPO_4 + 5AlPO_4 + 12H_2O$.

   This selective chemical etching targets the lithographic area where laser-written lines are present. The modified regions, exhibiting a different refractive index compared to the surrounding glass, dissolve at an accelerated rate relative to the unmodified areas. This dissolution discrepancy arises due to the contrast in optical properties.

   As a consequence of the etching process, air nanopores are generated within the laser-written lines, leading to the desired formation of a concentric pore ring structure. The dissolving of the modified regions and the subsequent formation of air nanopores are facilitated by the disparities in optical properties between the glass and air phases.

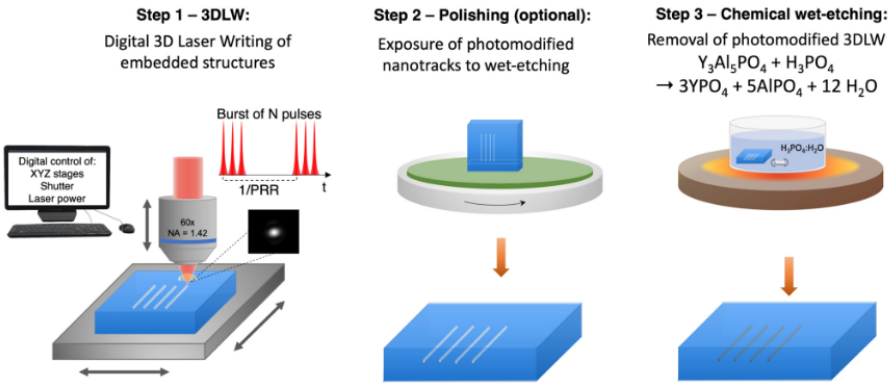


Figure 3: Schematic diagram of the 3D laser subtractive nanolithography process

### 6.5 Effect of Mode Field Distribution on Waveguide Coupling Loss

As previously indicated, one of the primary objectives of this research is to investigate the intricate interaction between an optical wave and a photonic crystal structure within the context of a conventional optical fiber having a MFD = 7.4 $\mu$m. A comprehensive analysis of the diverse categories of losses encountered in these systems is of utmost significance. These losses can be categorized into three distinct classes: input and output coupling losses between the waveguide and the photonic crystal, as well as propagation losses along the waveguide.

The losses due to propagation along the crystal will be studied through simulations of the fundamental modes of each of the structures using the *RSoft CAD: BeamPROP* program. However, it is important to note that this program does not consider losses caused by possible diffractions that may occur during propagation. Additionally, absorption losses of the material have not been taken into account in the initial analysis. The main reason for not including absorption losses in the simulations was that this study focused, in a preliminary approach, on analyzing losses caused by dispersion or radiation losses of the wave.

The *RSoft CAD: BeamPROP* program can estimate the losses occurring in the coupling, which is important for comparing them with the expected losses in this type of waveguide. It is known that the calculation of coupling losses between a single-mode waveguide and a single-mode fiber can be performed using the overlap integral, which involves the mode field radii of the fiber and the waveguide. However, calculating the coupling loss using this integral can be time-consuming and a simplified expression based on the Gaussian field approximation is often used. This approximation considers the coupling loss between a single mode fiber with a circular mode and a single mode waveguide [ref:11].

The simplified expression for the coupling loss is given by:

$$\frac{P_{Out}}{P_{In}} = \frac{4 \cdot (MFR_{Fiber})^2 \cdot (MFR_{\text{Wave guide}})^2}{((MFR_{Fiber})2 + (MFR_{\text{Wave guide}})^2)^2} \tag{13}$$

This approximation considers the coupling loss between a single mode fiber with a circular mode and a single mode waveguide. The parameters $MFR_{Fiber}$ and $MFR_{\text{Wave guide}}$ correspond to the mode field radius of the fiber and the mode field radius of the waveguide mode, respectively.

## 6.6 *RSoft CAD* waveguide simulation software program

The *RSoft CAD* environment [ref:12] is a highly useful program that enables the creation of systems for the design of waveguide devices, optical circuits, and other photonic devices. It serves as a control program for various passive device modules within the *RSoft* software suite, such as *BeamPROP*.

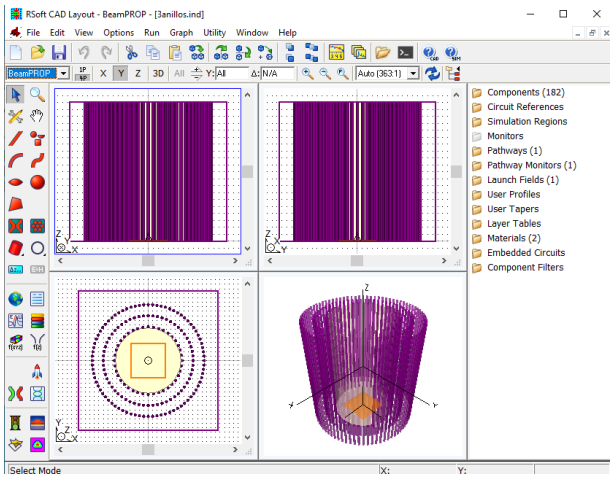


Figure 4: Multi-pane view of 3D CMOS design in CAD showing views along the X, Y, and Z axes as well as a 3D view.

The *RSoft CAD* environment is specifically designed for photonic devices and circuits, offering a wide range of essential components, including lines, cones, curves, lenses, and polygons, which can be selected and added through a graphical interface. Additionally, it allows for the creation of customized components using mathematical equations or data files. These components can be configured with specific properties, such as shape and optical characteristics, using arithmetic expressions that incorporate user-defined variables.

In addition to the aforementioned components, the *RSoft CAD* environment offers 3D editing capabilities, multi-pane view options for simultaneous display of different perspectives, and an object-oriented design environment that facilitates the construction of complex structures using smaller components.

In the context of photonic crystals, *RSoft CAD* proves particularly valuable as it enables the modeling of electromagnetic wave propagation in periodic structures. It offers tools for generating periodic geometries, such as the creation of unit cells, which are crucial for effective study of these systems.

Now that we have discussed the general capabilities of *RSoft CAD*, we can now focus on the specific module used in this study, which is *BeamPROP*.

### 6.6.1 RSoft CAD: BeamPROP

*BeamPROP* [ref:13] utilizes the finite difference beam propagation method to simulate the propagation of light waves in waveguides with various geometries. This method relies on parabolic approximations of the Helmholtz equation. However, it is important to note that this approach has certain limitations, such as considering scalar waves and adhering to the paraxiality condition.

To address these limitations, *BeamPROP* offers more advanced techniques, including vector beam propagation that takes into account polarization effects. The program also features a bidirectional algorithm (BPM: BeamPROP Method), enabling the consideration of both forward and backward propagating waves, including reflections.

To utilize *BeamPROP*, two essential elements need to be provided: the refractive index distribution and the input wavefield. With this information, the program determines the wavefield in the remaining domain of interest. Additionally, it allows adjustment of numerical simulation parameters such as computational domain size, grid dimensions, and longitudinal pitch.

The BPM approach employed by *BeamPROP* focuses on approximations and numerical solutions of the wave equation specifically for monochromatic waves. Under the assumptions of a scalar field (ignoring polarization effects) and paraxiality (limiting the propagation to a narrow range of angles), the problem is formulated, and the simulation is performed based on the underlying methodology.

In the context of monochromatic waves, the wave equation takes the form of the well-known Helmholtz equation:

$$\begin{cases} \frac{\partial^2 \mu}{\partial x^2} + \frac{\partial^2 \mu}{\partial y^2} + \frac{\partial^2 \mu}{\partial z^2} + k(x,y,z)^2 \cdot \mu = 0 \\ \\ \mu(x,y,z) = u(x,y,z) \cdot e^{i \cdot \bar{k} \cdot z} \end{cases} \tag{14}$$

The scalar electric field is given by the equation: $E(x,y,z,t) = \mu(x,y,z) \cdot e^{(-i\omega t)}$, $E$ represents the electric field. The wavenumber $k$ is defined as: $k = \frac{2\pi}{\lambda}$, here $\lambda$ is the wavelength in free space. In this context, we use $\bar{k}$ as a constant that represents the average phase variation of the $\mu$ field and is known as the reference wavenumber. The problem formulation focuses on the spatial variables $x$, $y$, and $z$.

In typical guided wave problems, the fastest variation in the $\mu$ field is associated with the phase variation resulting from propagation along the guide axis. Assuming that the guide axis is predominantly in the $z$-direction, it is advantageous to decompose this rapid variation by introducing an additional field called the "slow variation field." The second equation in the set of Equations 14 represents this decomposition, where $\mu(x,y,z)$ is expressed as the product of the slow variation field $u(x,y,z)$ and the exponential factor $e^{i \cdot \bar{k} \cdot z}$.

By substituting the second equation into the Helmholtz equation, we obtain the following expression for the slowly varying field:

$$\frac{\partial^2 u}{\partial z^2} + 2i\frac{\partial u}{\partial z} + \frac{\partial^2 u}{\partial x^2} + \frac{\partial^2 u}{\partial y^2} + (k^2 - \bar{k}^2)u = 0 \tag{15}$$

At this stage, the equation provided above is equivalent to the exact Helmholtz equation, but expressed in terms of the slowly varying field $u$. We make the assumption that the variation of $u$ with respect to $z$ is sufficiently slow that the first term in the equation can be neglected compared to the second term. This approximation is commonly known as the slowly varying envelope approximation, or alternatively, the paraxial approximation or parabolic approximation. With this assumption and a slight rearrangement, the equation simplifies to:

$$\frac{\partial u}{\partial z} = \frac{i}{2\bar{k}}\left(\frac{\partial^2 u}{\partial x^2} + \frac{\partial^2 u}{\partial y^2} + (k^2 - \bar{k}^2)u\right) \tag{16}$$

This equation serves as the fundamental equation for the Beam Propagation Method (BPM) in three-dimensional (3D) simulations. Given an input field, u(x, y, z=0), the equation determines the field's evolution in the space for z>0.

The resulting equation represents a parabolic partial differential equation, which can be solved using methods such as the Fourier split-step method or the Crank-Nicholson scheme [ref:13]. These numerical techniques account for specific boundary conditions established in the simulation, enabling accurate solutions for the given problem.

Moreover, the program offers methods that surpass the paraxial limitations and enable more precise calculations in scenarios with large angles and index contrasts. This extends the program's capabilities to analyze situations that demand a broader approach beyond paraxial propagation.

Furthermore, the program utilizes advanced computational algorithms to calculate the modes of wave propagation in a user-designed structure. It takes into consideration the appropriate boundary conditions, allowing for the determination of both the fundamental mode and higher-order modes. By solving the governing equations numerically, the program determines the spatial distribution and characteristics of each mode within the structure.

The calculated modes of wave propagation within the user-designed structure can be further visualized and analyzed using the powerful visualization tool called *WinPLOT*.

### 6.6.2 WinPLOT

*WinPLOT* [ref:14] is a technical graphics package that is utilized in conjunction with the *RSoft Photonic Device Tools*. It is a versatile graphing application designed to visualize scientific results stored in ASCII data files. It specifically excels in displaying cross-sectional profiles of fundamental modes that are calculated using the *RSoft BeamPROP* module. *WinPLOT* supports various platforms, making it compatible across different operating systems. Its primary purpose is to provide an intuitive and effective means of graphically representing and analyzing scientific data in the context of photonic device simulations.

In addition to its graphical capabilities, WinPLOT offers a command line interface that enables users to analyze and manipulate the data being plotted. This command line functionality empowers users to perform various operations, calculations, and transformations on the data prior to visualization. By utilizing the command line, users can apply filters, interpolate data, adjust parameters, and conduct other data analysis tasks. This feature enhances the flexibility and control over data presentation and processing, enabling users to customize and refine their analysis according to their specific requirements.

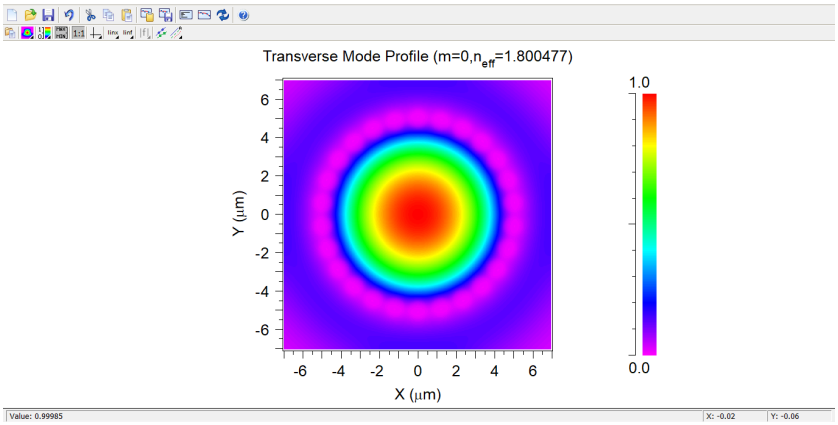


(a) Image of the field distribution of the fundamental mode for a structure composed of a 10 $\mu$m diameter ring with 26 pores, as depicted in the *WinPLOT* program.

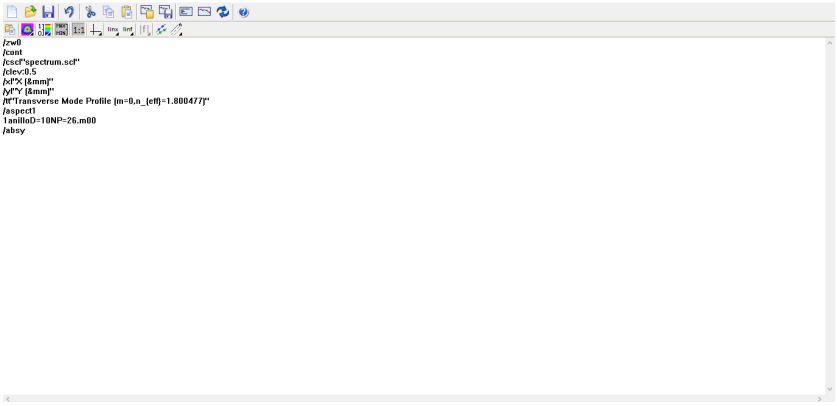


(b) Command line interface in the *WinPLOT* program.

Figure 5: Image and command line interface in the *WinPLOT* program.

## 6.7 Explanation of the structures simulated by the program

The objective of this study is to investigate different structures formed by concentric rings of pores under various configurations. To achieve this, multiple structures were formed based on two different criteria:

### 6.7.1 First Group of Structures

In this first group, we conducted a study on structures composed of three concentric rings that met several essential conditions:

- It was established that each ring should consist of at least 8 circular pores of 1 $\mu$m diameter.
- To generate additional structures, the number of pores in each ring was increased while ensuring that the inter-pore spacing (which is the distance between the centers of two distinct pores) remained constant within each ring, until reaching a point where no more pores could be added without overlapping.
- The decision was made to explore structures with varying core diameters, namely 10, 11, 12,

13, 14, and 15 $\mu$m. The core diameter is defined as the distance from the center of the guide to the center of one of the pores in the first ring.

- Each pore ring was to be 5 $\mu$m larger in diameter than the previous ring.

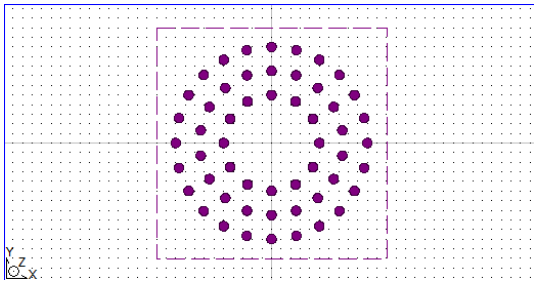

Figure 6: Structure of 3 rings formed by pores with equal inter-pore spacing of 2.61799 $\mu$m in all the rings

In addition to the structures mentioned above, we also studied structures that met the exact same configurations but with two and one ring.

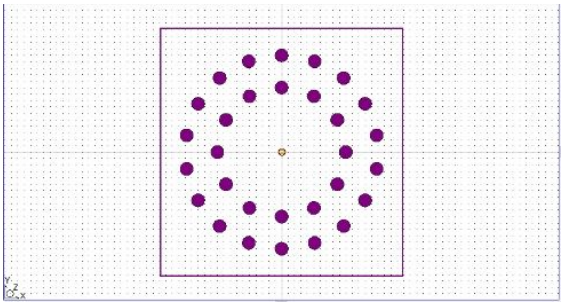

(a) Structure of 2 rings formed by pores with equal inter-pore spacing of 2.61799 $\mu$m in all the rings

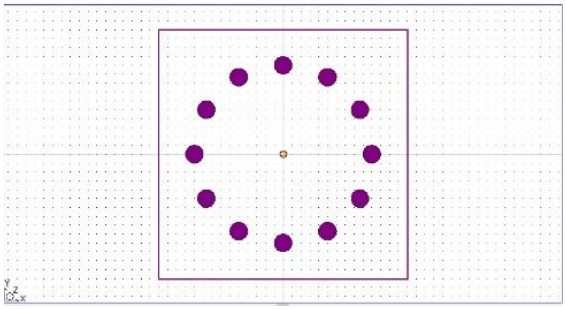

(b) Structure of 1 ring formed by pores with equal inter-pore spacing of 2.61799 $\mu$m

Figure 7: Structures with different numbers of rings and equal inter-pore spacing

However, due to the limitations imposed by this criterion, the number of structures that could be investigated was significantly reduced. In order to increase the diversity of structures studied, an additional configuration was explored.

### 6.7.2 Second Group of Structures

In the second case, we explored a broader range of scenarios by maintaining a constant distance between pores within the same ring, although it may differ from the distance between pores in different rings, while still being similar. This approach allowed for a more diverse analysis. The following procedure was followed:

- Initially, a laser propagation simulation was conducted in a single circular ring with a diameter of 10 $\mu$m. This ring consisted of 8 evenly spaced circular pores, each with a diameter of 1 $\mu$m.

- The number of pores in each ring was gradually increased by adding 2 more pores at each step. This incremental increase was chosen to prevent pore overlap and ensure accurate simulations.
- The process of adding more pores in each ring continued until reaching a point where it was no longer feasible to add additional pores without causing overlap between them.

By following this procedure, we were able to systematically explore the behavior and characteristics of the photonic crystal structures with varying numbers of pores within each ring.

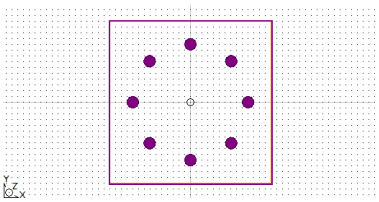

(a) Ring formed by 8 pores with a diameter of 10 $\mu$m

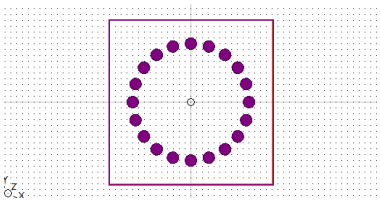

(b) Ring formed by 20 pores with a diameter of 10 $\mu$m

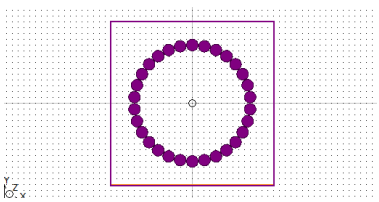

(c) Ring formed by 30 pores with a diameter of 10 $\mu$m

Figure 8: Examples of rings with different numbers of pores

Subsequently, the diameter of the ring was increased by 1 $\mu$m and the same procedure was repeated until a diameter of 15 $\mu$m was reached.

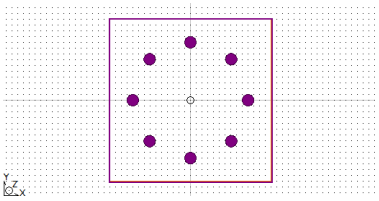

(a) Ring consisting of 8 pores of 10 $\mu$m in diameter

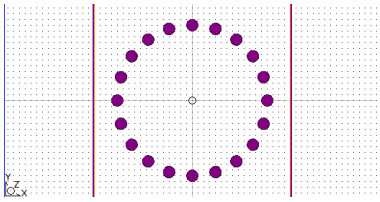

(b) Ring consisting of 20 pores of 13 $\mu$m in diameter

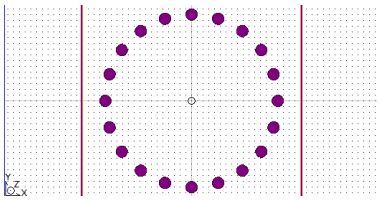

(c) Ring consisting of 20 pores of 15 $\mu$m in diameter

Figure 9: Examples of rings with different numbers and diameters of pores

Once a diameter of 15 $\mu$m was reached in the second case, an additional pore ring was added to the structure, always with a diameter 5 $\mu$m larger than the diameter of the first ring.

After adding the new ring, the central ring was configured with 8 pores, while the newly added outer ring was configured with 12 pores. This configuration ensured that there was a difference in the distance between the pores of the two rings, while still maintaining approximate values.

Pores were then added to the outer ring in groups of 3, following the same procedure as described above, until it was no longer possible to add more pores without causing overlap. This procedure allowed for an incremental increase in the number of pores in the outer ring while maintaining a controlled difference in pore spacing between the two rings.

As the diameters of the two rings increased, the difference in pore spacing also increased. However, by following the above procedure, it was ensured that the difference between the pore spacing of the rings did not exceed 1 $\mu$m. This criterion helped maintain a consistent and manageable

structure for analysis while exploring a wider range of configurations.

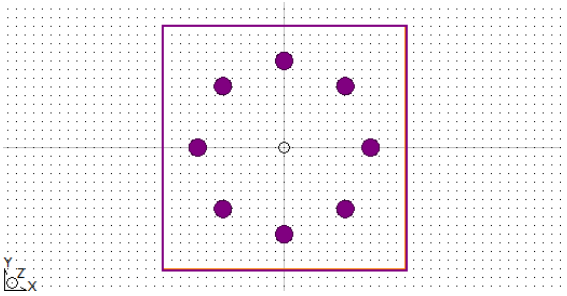

(a) Simulated structure composed of only one ring

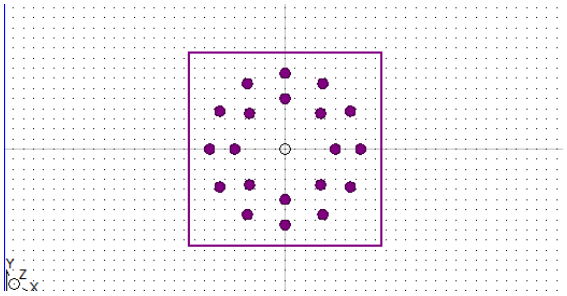

(b) Simulated structure composed of two rings

Figure 10: Examples of simulated structures with different numbers of rings

This process was repeated until a structure with three concentric rings was obtained, as this is the structure that the laser laboratory is trying to fabricate. Once the third ring was added, the first ring was reconfigured with 8 pores, the second ring with 12 pores and the third ring with 16 pores, increasing by 4 pores each time to keep the maximum difference between the pore distances of the different rings below 1 $\mu$m.

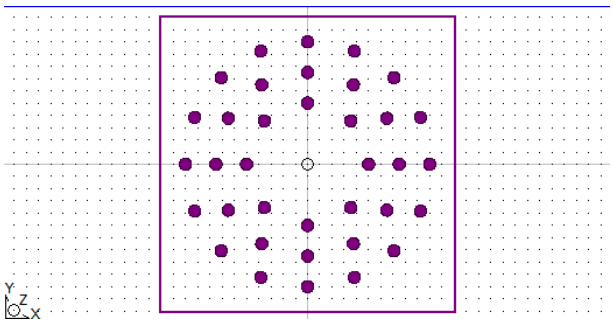

Figure 11: Simulated structure composed of three rings.

### 6.7.3 Criterion used to study the distribution of the electric field of the modes.

In the first part of this work, we study how the electric field distribution of the fundamental mode varies for the structures described in the previous section. For this we use the program *WinPLOT*, which can represent the field distribution:

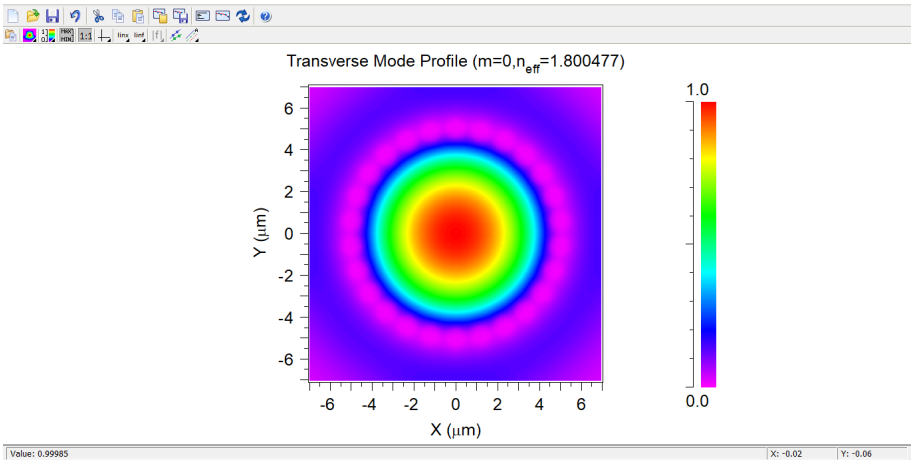


Figure 12: Transverse distribution of the amplitude of the fundamental mode electric field of a single 26-pore ring structure with a core diameter of 10 $\mu$m

In order to study the fundamental mode distribution for the type of structures being simulated, a method was proposed to measure the diameter at which the electric field amplitude distribution reaches the value of $1/e$ (D[$1/e$]). With this parameter, an analysis of the mode field distribution among different structures is possible, enabling the observation of the parameters that affect this distribution.

To measure this diameter, the program can generate a contour within the mode field representation comprised of points that have a value equal to a specified one. In our specific case, we create a contour that encompasses data with a value of $1/e$:

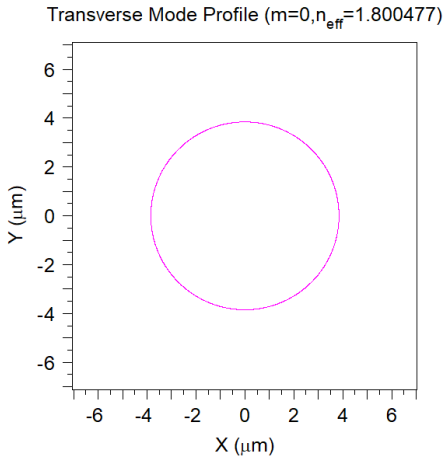


Figure 13: Contour created for values equal to $1/e$ for the transverse distribution of the amplitude of the fundamental mode electric field of a single 26-pore ring structure with a core diameter of 10 $\mu$m.

And, with the assistance of the status bar located at the bottom of the *WinPLOT* window, which displays the mouse coordinates, the diameters D[$1/e$] of the fundamental modes were determined.

However, it was observed that not all modes exhibit a clear Gaussian distribution. This is evident in the case of structures composed of 2 ring-shaped pore arrays, with a central ring of 10

pores and an outer ring of 15 pores, with a core diameter of 10 $\mu$m. The fundamental mode field distribution for this structure displayed irregularities:

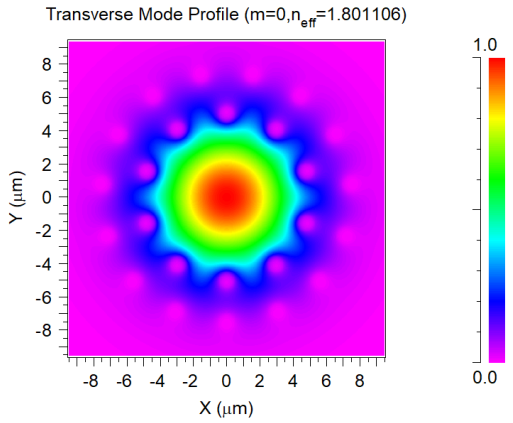


(a) Distribution of the electric field for the fundamental mode in a simulated structure composed of 2 ring-shaped pore arrays, with a central ring of 10 pores and an outer ring of 15 pores, with a core diameter of 10 $\mu$m

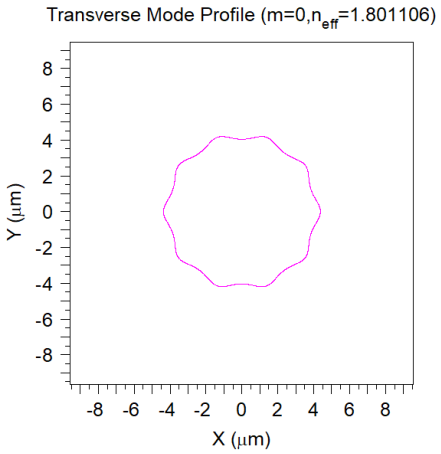


(b) Contour plot created for values equal to $1/e$ for a structure composed of 2 ring-shaped pore arrays, with a central ring of 10 pores and an outer ring of 15 pores, with a core diameter of 10 $\mu$m

Figure 14: Transverse distribution of the amplitude of the fundamental mode electric field with irregularities

To accurately capture the extent of mode field distributions exhibiting irregularities, such as the one shown, a suitable parameter was required. The diameter D[1/e] was employed as a measuring parameter to address this need. However, measuring a single diameter may not fully capture the overall size of the irregular distribution. To address this limitation, it was proposed to calculate the D[1/e] as the average of the major and minor diameters present in the contour. This approach accounts for any irregularities or asymmetries in the contour shape, providing a balanced estimate that encompasses the variability in dimensions. By considering both the maximum and minimum extents of the distribution, this method offers a comprehensive measurement of the mode field's overall size, ensuring a more accurate analysis of the fundamental mode behavior.

# 7 Results and discussion

En esta sección se presentan y discuten los resultados obtenidos de las simulaciones de las estructuras mencionadas anteriormente. En la primera parte, se analiza la variación del parámetro D[1/e] y la distribución del campo de los modos fundamentales obtenidos en la simulación en relación con el número de poros de la estructura, el arco entre poros, el diámetro del núcleo y el número de anillos presentes en la estructura. En la segunda parte, se examina el impacto de estos parámetros en la potencia transmitida y la formación de modos superiores al fundamental al propagar el modo fundamental en cada una de las estructuras. Además, se discuten y analizan los casos en los que la estructura está compuesta por un número elevado de poros, y se investigan los factores que influyen en la formación de modos superiores en este escenario. Por último, se analizan los resultados de las simulaciones de propagación de una onda Gaussiana con un MFD de 7.4 $\mu$m y se comparan con los resultados obtenidos en el caso anterior. También se observa un

efecto de saturación en el cual agregar más poros a la estructura o reducir el arco entre ellos no afecta significativamente la cantidad de potencia transmitida.

---

## 7.1 Fundamental modes of each structure

To accurately analyze the variation of the D[1/e] parameter for each structure, the following procedure has been followed. Firstly, the value of D[1/e] has been plotted for each of the simulated structures. In the case of the first group of structures, D[1/e] has been plotted with respect to the inter-pore spacing, while for the second group of structures, it has been plotted with respect to the number of pores in each ring. Once the data has been plotted, the variation of the D[1/e] parameter with respect to the number of pores, inter-pore spacing, core diameter, and number of rings in the structure has been analyzed.

To ensure a comprehensive analysis, the collected data has been visually presented through various plots according to the following configuration:

- The color assigned to each data point in the plot indicates the number of rings present in the corresponding structure, following the following rules:

| **Color** | **Number of rings** |
|---|---|
| **Black** | Structure formed by only one ring. |
| Red | Structure formed by two rings. |
| Blue | Structure formed by three rings. |

- Also, the points have different shapes to differentiate the size of the core in each case:

| **Shape** | **Core diameter** |
|---|---|
| Square: □ | 10 $\mu$m |
| Upward triangle: △ | 11 $\mu$m |
| Downward triangle: ▽ | 12 $\mu$m |
| Circle: ○ | 13 $\mu$m |
| Star: ☆ | 14 $\mu$m |
| Diamond: ◇ | 15 $\mu$m |

### 7.1.1 D[1/e] as a function of the inter-pore spacing

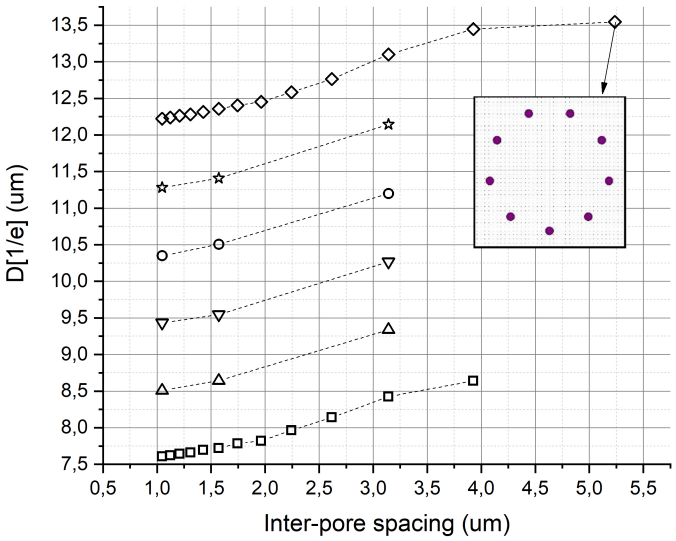


Figure 15: Single-ring structures

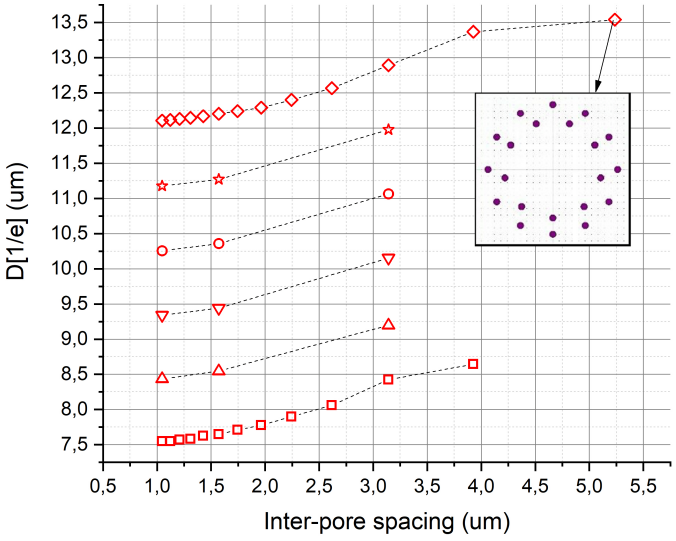


Figure 16: Two-ring structures

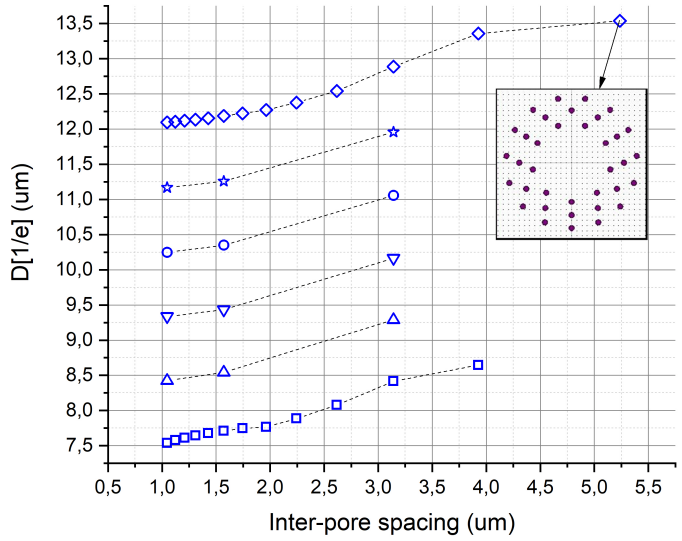


Figure 17: Three-ring structures

### 7.1.2 D[1/e] as a function of the number of pores in the structure

In the following plots, for structures with more than 1 ring, the number of pores for each ring was represented on the horizontal axis as follows: *Number of pores 1st ring / Number of pores 2nd ring / Number of pores 3rd ring.*

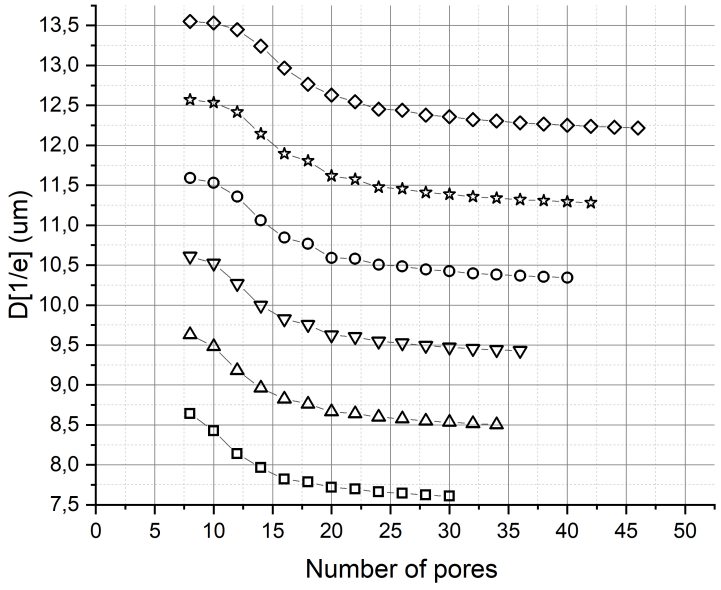


Figure 18: Single-ring structures

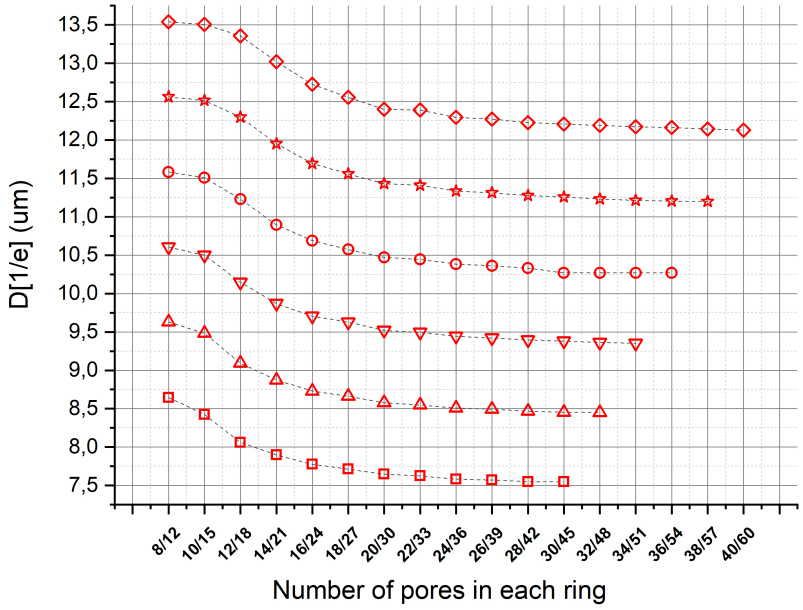


Figure 19: Two-ring structures

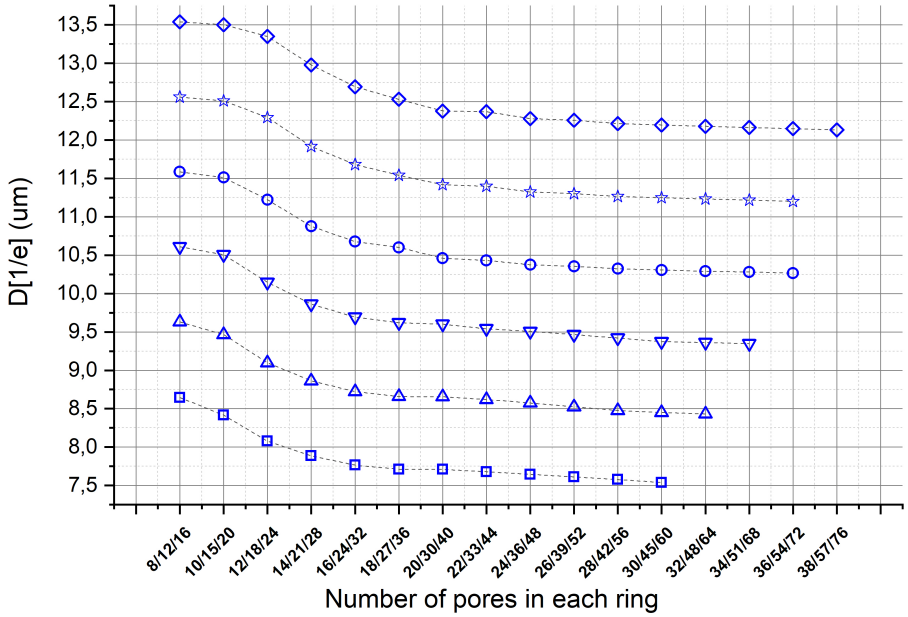


Figure 20: Three-ring structures

### 7.1.3 Variation of D[1/e] with respect to the inter-pore spacing and the number of pores in the structure.

Figures 15, 16, and 17 shown that as the inter-pore spacing increases, the value of D[1/e] also increases; indicating that the mode field distributions are spread more widely within the structure.

On the other hand, the figures 18, 19, and 20 reveal a similar behavior. It is observed that as the number of pores in the structure increases, and therefore the pore spacing of the ring decreases, the value of D[1/e] decreases asymptotically to a fixed value which depends on the diameter of the core. This aspect will be discussed in more detail in Section 7.1.4.

This trend suggests that as the number of pores in the rings increases (or equivalently, as the inter-pore spacing decreases), the wave becomes more confined within the core of the structure. As a result, the mode field distribution becomes narrower and approaches a Gaussian-like shape. In other words, as the structure becomes denser with pores, the mode field becomes localized closer to the center of the structure, generating a narrower and more symmetrical distribution.

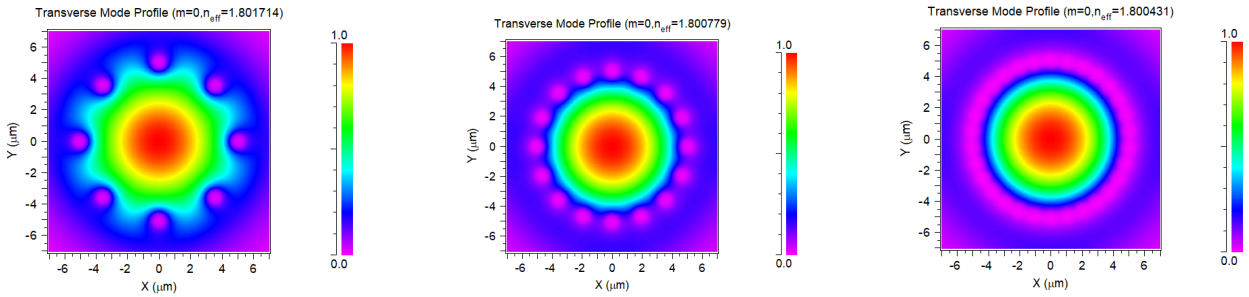


(a) Fundamental mode distribution for a structure with a single ring, 10 micrometers core and 8 equispaced pores

(b) Fundamental mode distribution for a structure with a single ring, 10 micrometers core and 16 equispaced pores

(c) Fundamental mode distribution for a structure with a single ring, 10 micrometers core and 30 equispaced pores

Figure 21: Fundamental mode distribution in different structures

### 7.1.4 Variation of D[1/e] with Core Diameter

As discussed in the previous section, a clear relationship between the core diameter and the fundamental mode parameter D[1/e] can be observed. To study this phenomenon in more detail, we will examine the variation of D[1/e] with respect to the diameter, considering two specific cases.Firstly, we will examine the behavior of D[1/e] when the inter-pore spacing is set at 1.0472 $\mu$m for a single-ring structure. This particular inter-pore spacing was chosen as it is one of the few values that is shared among structures with different core diameters. By conducting this investigation, we can gain insights into how the D[1/e] values are influenced by variations in the core diameter while keeping the inter-pore spacing constant.Subsequently, our investigation extends to single-ring structures characterized by a ring pore count of 30. Here, we examine how the D[1/e] values evolve as the core diameter varies while keeping the number of pores constant.

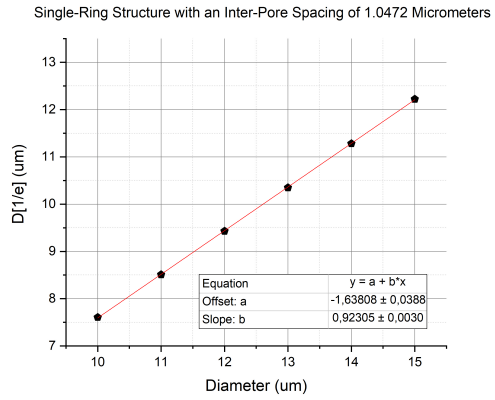


(a) Single-Ring Structure with an Inter-Pore Spacing of 1.0472 Micrometers

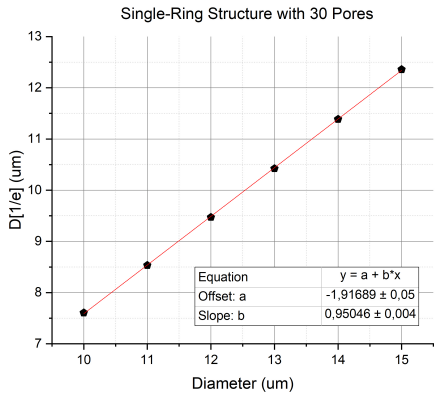


(b) Single-Ring Structure with 30 Pores

In both cases, a clear linear relationship between the parameter D[1/e] and the core diameter can be seen. This observation is intriguing, as it gives us the opportunity to perform a linear interpolation and compare the slopes of the lines in each case.

The calculated slope (b) for both cases exceeds the threshold of 0.9, indicating a strong positive correlation between the core diameter and the D[1/e] values. Specifically, for each structure, increasing the core diameter by 1 $\mu$m is associated with an approximate 1 $\mu$m increase in the corresponding D[1/e] value. This behavior aligns with the intuitive expectation that a larger core diameter allows for a greater amount of energy to be carried by the wave within the structure, resulting in a wider distribution of the field associated with the fundamental mode.

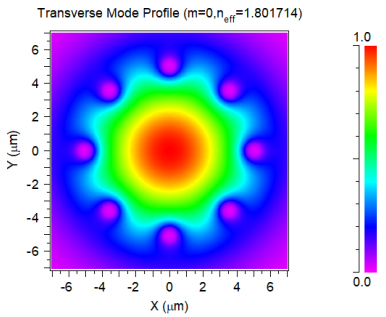


(a) Fundamental mode distribution for a structure with a single ring, 10 micrometer core, and 8 equispaced pores.

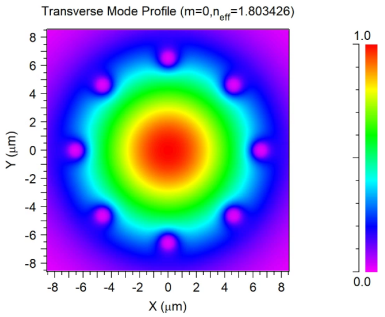


(b) Fundamental mode distribution for a structure with a single ring, 13 micrometer core, and 8 equispaced pores.

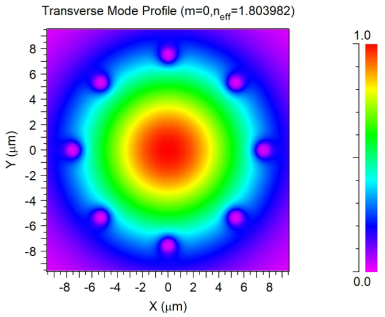


(c) Fundamental mode distribution for a structure with a single ring, 15 micrometer core, and 8 equispaced pores.

Figure 23: Fundamental mode distribution in different structures with different diameter core

### 7.1.5 Variation of D[1/e] with respect to the number of rings

The analysis of the obtained data reveals an interesting finding: there is no significant variation in the values of D[1/e] with respect to the number of rings in the structure. This result suggests that the distribution of the mode field is primarily determined by the first ring of pores, which forms the core of the structure. While additional rings contribute to the propagation of the wave within the structure, they do not have a noticeable impact on the distribution of the fundamental mode field.

This observation highlights the critical role of the core structure in shaping the mode field distribution. The first ring of pores establishes the fundamental characteristics of the field, while subsequent rings primarily assist in the wave propagation and overall structure stability. It is worth noting that the lack of significant variation in D[1/e] with increasing numbers of rings implies that the core structure's properties play a dominant role in defining the mode field distribution.

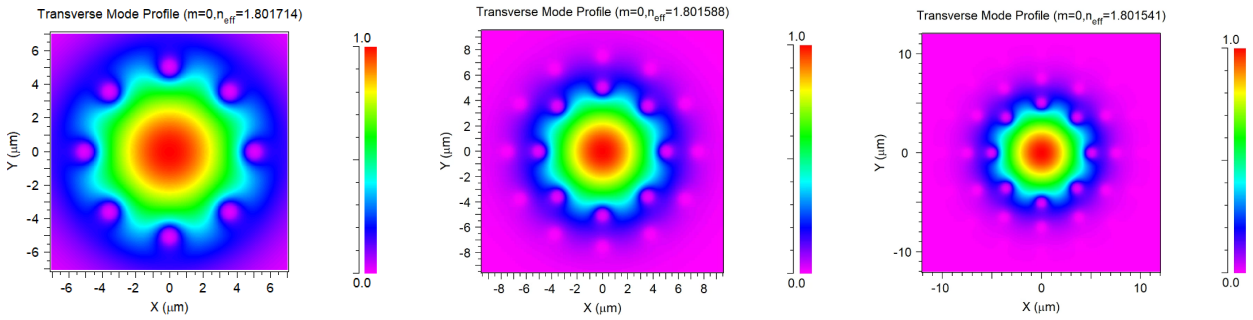


(a) Fundamental mode distribution for a structure with a single ring and 8 equispaced pores

(b) Fundamental mode distribution for a structure with 2 rings and a pore configuration of 8/12

(c) Fundamental mode distribution for a structure with 3 rings and a pore configuration of 8/12/16

Figure 24: Fundamental mode distribution in different structures with varying number of rings

## 7.2 Results of the Propagation of the Fundamental Mode in Each Structure

Once the fundamental modes of each structure have been obtained, their propagation through their respective structures has been simulated in order to analyze power losses during propagation and the potential formation of higher-order modes beyond the fundamental mode. The representation of the results follows the same criteria as outlined in Sections 7.1.1 and 7.1.2:

### 7.2.1 Normalized transmitted power as a function of the inter-pore spacing

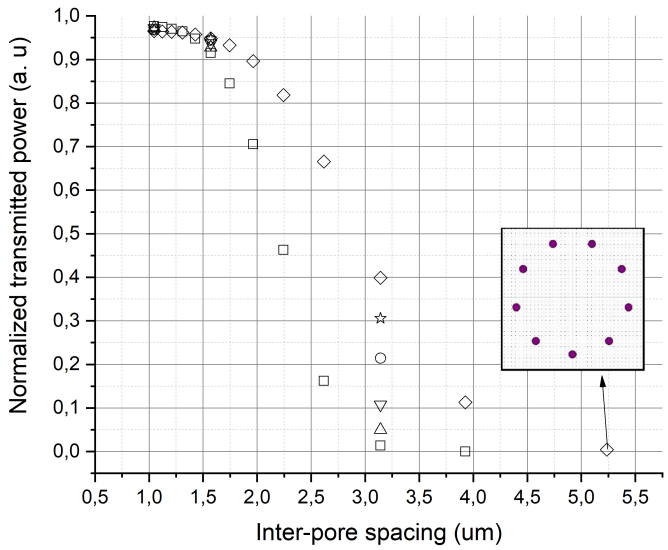


Figure 25: Single-ring structures

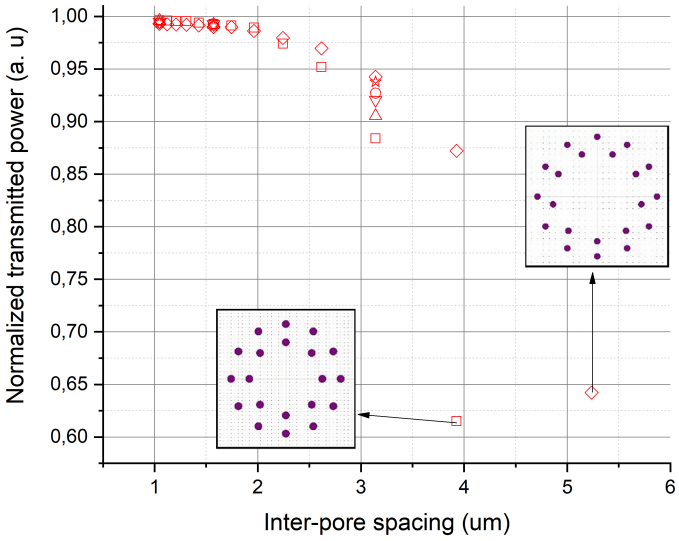


Figure 26: Two-ring structures

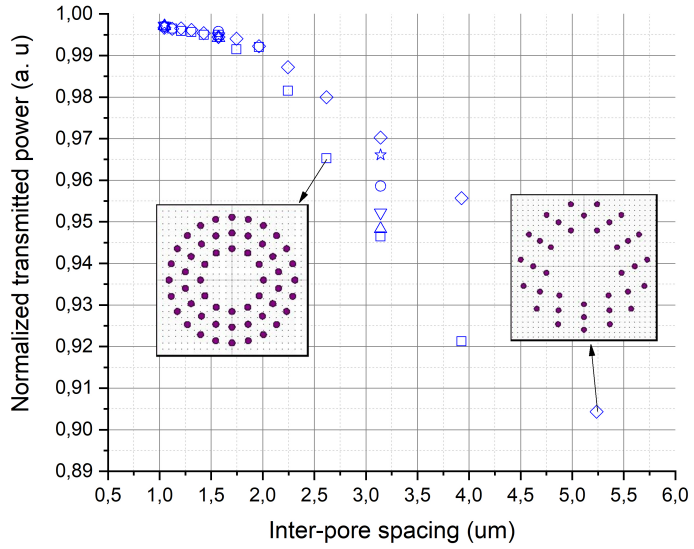


Figure 27: Three-ring structures

### 7.2.2 Normalized transmitted power as a function of the number of pores in the structure

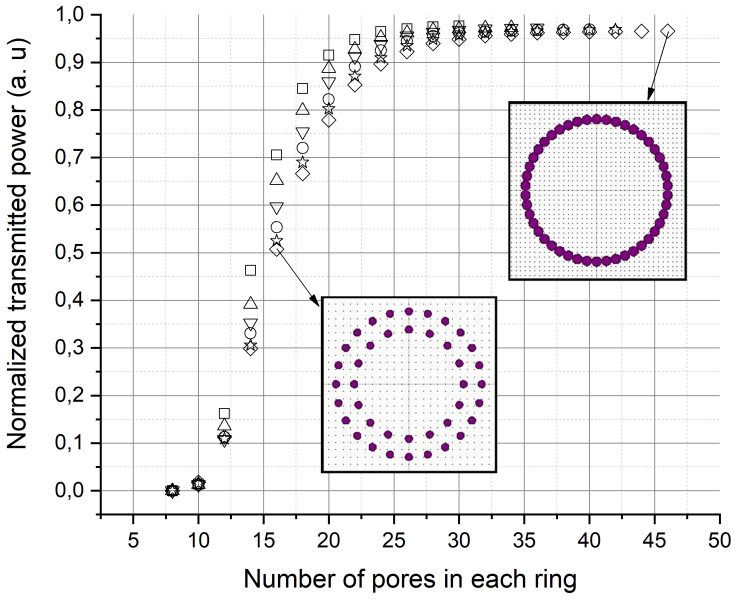


Figure 28: Single-ring structures

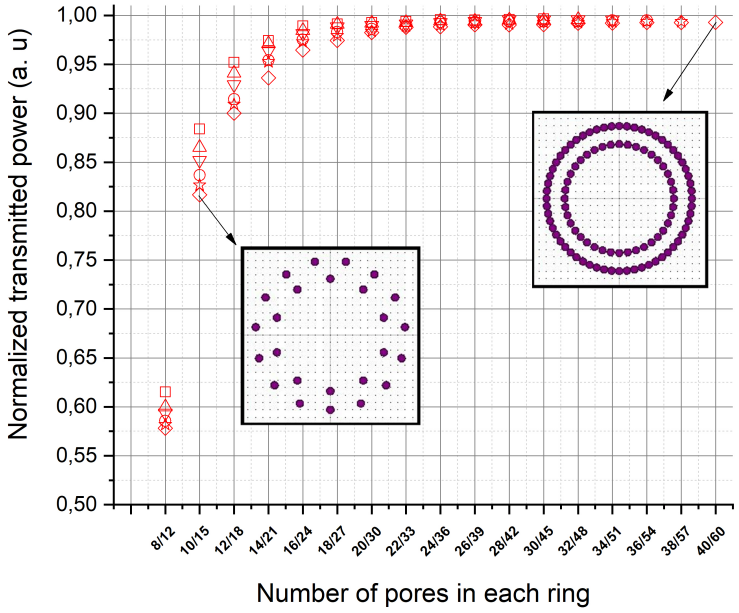


Figure 29: Two-ring structures

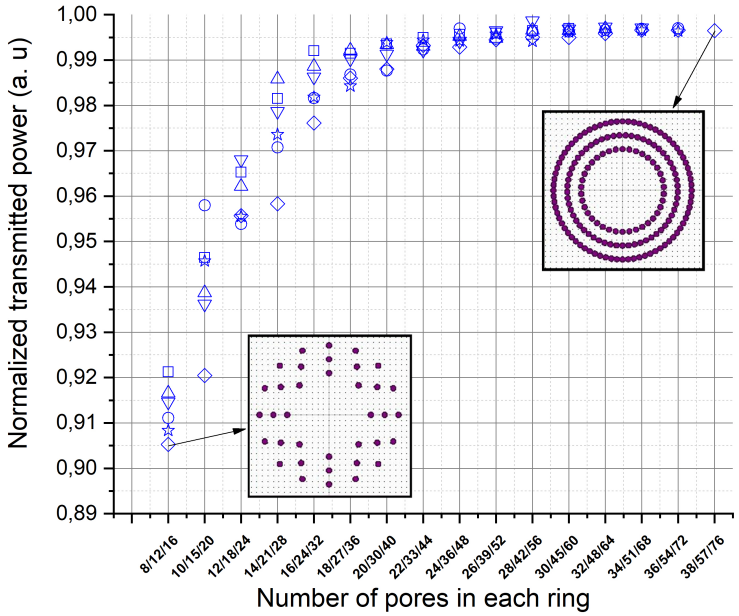


Figure 30: Three-ring structures

### 7.2.3 Impact of Number of Pores and Inter-Pore Spacing on the Propagation of Fundamental Modes in the Structures

The graphs depicted in Figures 25, 26, and 27 demonstrate a noticeable decrease in the transmitted power of the structures as the pore spacing increases. This behaviour can be attributed to the phenomenon of energy leakage through the pore spaces during wave propagation. As the pore

spacing increases, some of the wave energy escapes through these spaces, resulting in a reduction of the total power transmitted by the structure. Conversely, a decrease in pore spacing has a positive effect on wave propagation. With a smaller pore spacing, the probability of energy leakage decreases, thus favouring efficient wave propagation within the crystalline structure.

This effect would also explain why increasing the number of pores in each ring increases the amount of transmitted power as shown in Figures 28, 29, and 30. In this case, a higher number of pores in the rings favours the propagation of the wave, avoiding the appearance of losses. This is because a higher number of pores in the rings corresponds to a lower inter-pore spacing, which prevents part of the wave energy from leaking out of the structure, keeping it confined within the core.

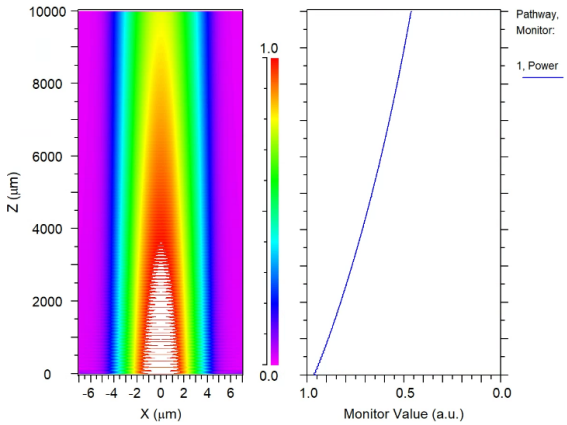


(a) Propagation of the fundamental mode in the XZ plane for a structure with a single ring, 10 micrometers core and 14 equispaced pores.

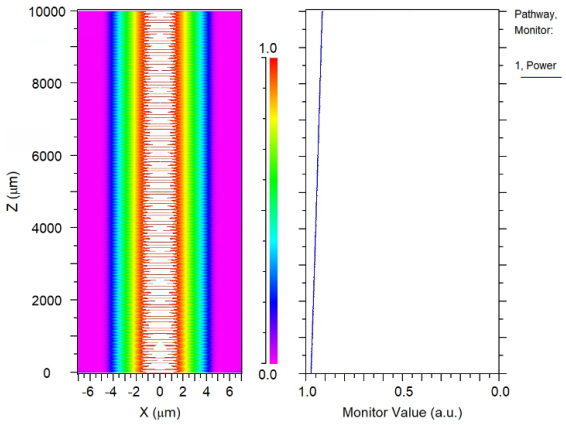


(b) Propagation of the fundamental mode in the XZ plane for a structure with a single ring, 10 micrometers core and 20 equispaced pores.

Figure 31: Propagation of the fundamental modes in different structures.

However, forming structures with a low inter-pore spacing (or with a large number of pores) implies that, although it improves the ability to propagate waves with minimal losses, it would also decrease the ability of these structures to eliminate higher-order modes beyond the fundamental mode, as discussed in Section 6.3.1. As the inter-pore spacing is reduced, the structure increasingly resembles an optical fiber, with a core made of Er:YAG crystal and a cladding with a refractive index equal to that of air. Thus, the waves propagating through these structures would propagate in a similar manner to how they would in a fiber, through total internal reflections, thereby favoring the formation of higher-order modes and eliminating the crystal's ability to eliminate higher-order modes that would form within the structure, as they could also propagate within the crystal without being eliminated. To analyze this effect, we will examine the propagation in the XZ plane for 3-ring structures with a core diameter of 10 $\mu$m, using the following pore number configurations: 8/12/16, 12/18/24, and 16/24/32:

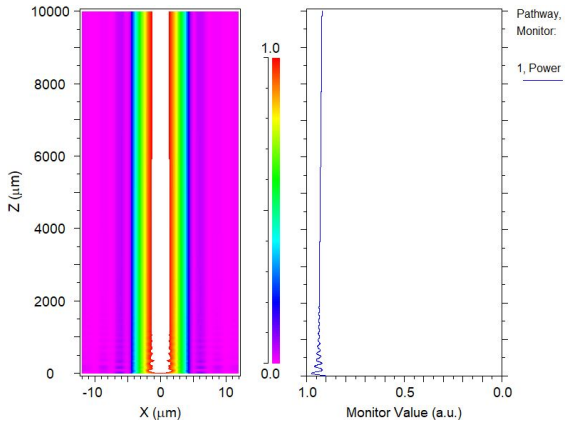


(a) Propagation in the XZ plane of the fundamental mode for the structure with the configuration 8/12/16

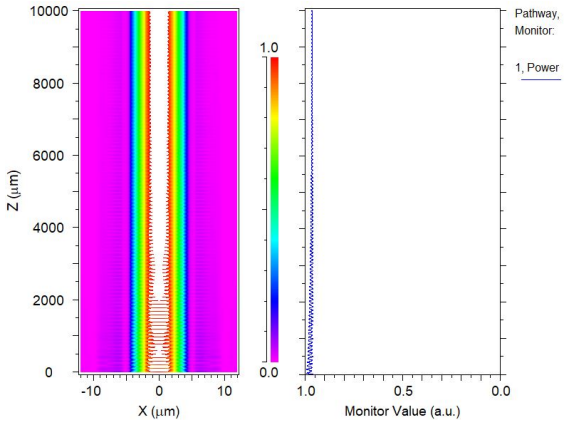


(b) Propagation in the XZ plane of the fundamental mode for the structure with the configuration 12/18/24

Figure 32: Propagation of the fundamental mode in different structures

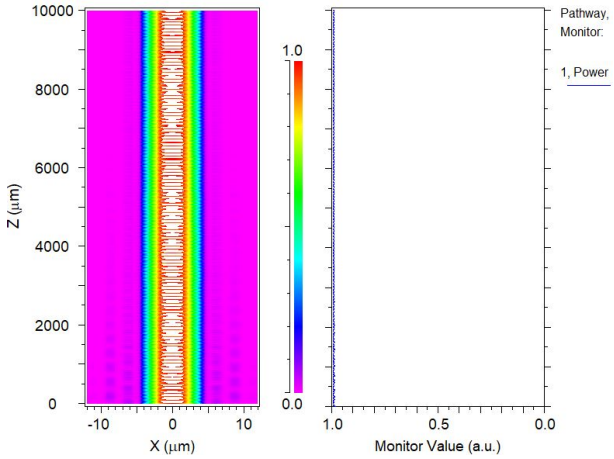


Figure 33: Propagation in the XZ plane of the fundamental mode for the structure with the configuration 16/24/32

In the previous figures, the mode distribution along the XZ plane for each structure is observed. The figures show certain perturbations or ripples in the wave distribution along the propagation, indicating that the wave has excited higher-order modes beyond the fundamental mode. In Figure 32a, we can see that these excitations occur at the beginning, but they do not reoccur as the propagation progresses. On the other hand, in Figure 33, these oscillations occur throughout the entire wave propagation, indicating the effect mentioned earlier. This indicates that not only adding pores to the structure (or equivalently reducing the inter-pore spacing) promotes the formation of higher-order modes, but these modes are not eliminated by the structure and can propagate through it. This is due to the fact that as the number of pores increases or the inter-pore spacing decreases, the propagation of an electromagnetic wave through the core follows the principles of optical fiber, relying on total internal reflections, rather than behaving like in a photonic crystal.

Thus, controlling and minimizing the pore spacing is crucial to maximize the transmitted power and optimize the performance of photonic crystal structures. However, it also promotes the formation and propagation of higher-order modes, eliminating the main property of these photonic crystal structures. Additionally, the fabrication process of these structures requires a great deal

of technical expertise, especially when dealing with small inter-pore spacing or a high number of pores within a ring. These conditions can increase the risk of crystal fracture, further complicating the manufacturing process.

However, the wave propagation is not only affected by the inter-pore spacing, but we also observe dependencies on the core diameter and the number of rings. These dependencies will be studied in more detail in Sections 7.2.4 and 7.2.5, respectively.

Furthermore, in Figure 32a, it can be observed that the distribution of the electromagnetic field exhibits an phenomenon known as the Top Flat effect during its propagation [ref:15].

### 7.2.4 Impact of Core Diameter on propagation of the fundamental modes in the structures

The amount of power transmitted by the structure is also affected depending on the core size, as observed in the data. In the figures 25, 26, and 27, an increase in the core diameter is associated with an increase in transmitted power. However, in Figures 28, 29, and 30, the opposite effect is observed, where an increase in the core diameter leads to a decrease in transmitted power. This may appear contradictory, but it is not.

To resolve this apparent contradiction, we will examine how the transmitted power varies with the core diameter for two different cases. In the first case, we study the variation of transmitted power for single-ring structures with a fixed inter-pore spacing of 3.14 $\mu$m. In the second case, we also analyze the variation of transmitted power with respect to the core diameter for single-ring structures with a fixed number of 20 pores:

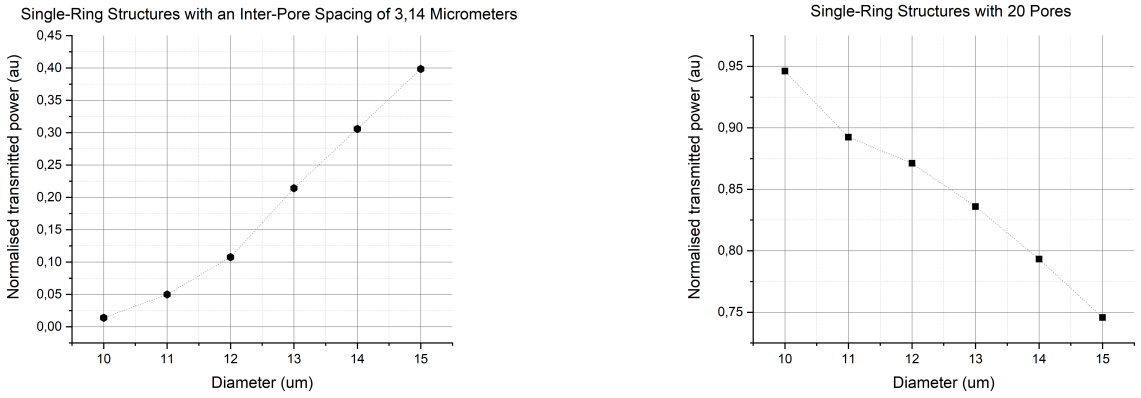


(a) Power versus core diameter for an inter-pore spacing of 3.14 micrometers

(b) Power versus core diameter for a number of pores equal to 20

Figure 34: Power Variation with Core Diameter for Different Parameters

Figure 34a demonstrates a clear positive correlation between the transmitted power and the core diameter. This correlation can be attributed to the concentration of energy within structures possessing larger core diameters. In such cases, the modes of the wave are concentrated primarily at the center of the core, distant from the ring of pores. Consequently, the leakage of energy through the pores is impeded, leading to improved propagation. Conversely, cores with smaller diameters encounter more pronounced energy losses as a result of increased interaction between

the wave and the pores.

However, in Figure 34b, we observe the opposite effect. How is this possible?. This difference from the previous case is due to the fact that, while keeping the number of pores constant, increasing the core diameter also increases the inter-pore spacing, leading to higher losses generated by the structure due to wave energy leaking through the inter-pore spacing. Therefore, although a larger core could retain more of the wave energy inside it, this effect is counteracted by the increase in losses, resulting in the observed outcome in Figure 34b.

However, it is also evident from Figures 25, 26, and 27, 28, 29, and 30 that this variation in transmitted power with respect to the core diameter for both cases becomes insignificant when increasing the number of pores in the structure (or equivalently, decreasing the inter-pore spacing) or the number of rings.

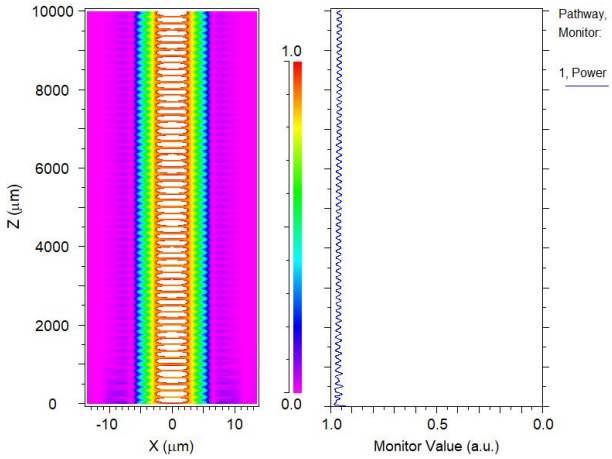


Figure 35: Propagation of the fundamental mode in the 3-ring structure with a core diameter of 13 $\mu$m and a pore configuration of 12/18/24

By comparing the previous figure with Figure 32b, we observe that the latter exhibits fewer oscillations and disturbances, which shows oscillations throughout its propagation. This suggests that a larger core diameter allows for the formation and propagation of a greater number of higher-order modes beyond the fundamental mode, similar to what occurs in optical fibers.

### 7.2.5 Impact of Number of Rings on propagation of the modes in the structures.

To investigate the relationship between the number of rings and transmitted power, we will analyze how the transmitted power varies with the number of rings for structures with pore configurations of 8, 8/12, and 8/12/16 pores in each ring, considering different core diameters:

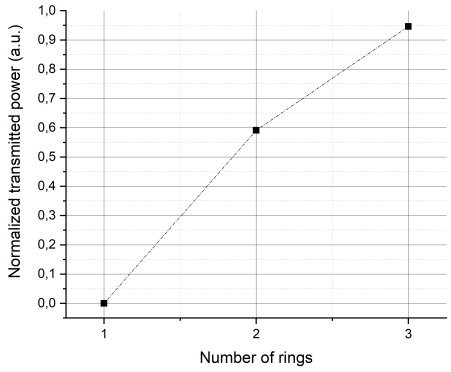


(a) Transmitted power as a function of the number of rings for a core diameter of 10 $\mu$m

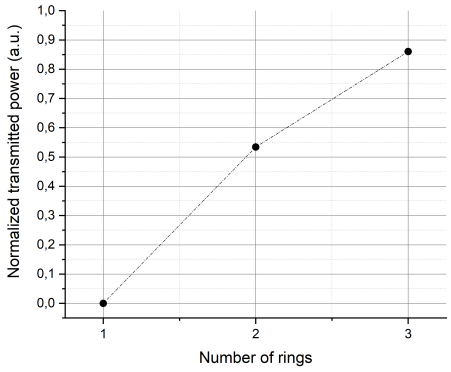


(b) Transmitted power as a function of the number of rings for a core diameter of 13 $\mu$m

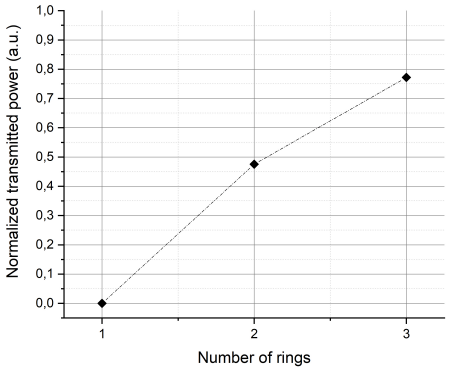


(c) Transmitted power as a function of the number of rings for a core diameter of 15 $\mu$m

Figure 36: Transmitted power variation with number of rings for different core diameters

As can be seen in Figures 36a, 36b and36c; an increase in the number of rings in the structure implies an significante increase in the transmitted power. This is because, as the number of rings in the structure increases, less wave energy is filtered through the structure, and more of it remains confined within the core. However, as shown in Figures 25, 26,27,28,29 and 30; the incremental increase in transmitted power due to the number of rings becomes smaller as the number of pores increases or the inter-pore spacing decreases. This is because, in this case, the central ring has a more significant influence on wave propagation than the outer rings.

As discussed in Section 7.2.3, forming structures with a low inter-pore spacing (or structures with a large number of pores) presents great difficulty due to the potential appearance of defects or breaks in the crystal during formation. Therefore, the results obtained in this section are particularly interesting since by adding multiple rings around the core, we increase the amount of transmitted power while maintaining an inter-pore spacing value that prevents the formation of defects in the crystal.

Regarding the formation of higher-order modes, we will analyze the impact of increasing the number of rings on their formation. Therefore, we will investigate how the number of rings affects the propagation of the fundamental mode for the structures with the pore configurations described above, considering a core diameter of 10 $\mu$m. The structure with the pore configuration 8/12/16

is already shown in Figure 32a.

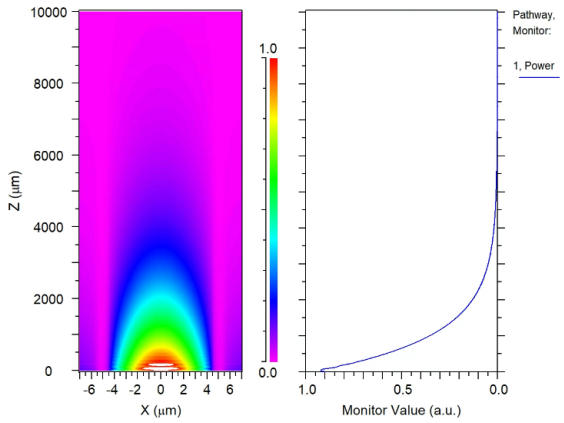


(a) Propagation of the fundamental mode for a structure composed of 1 ring formed by 8 pores

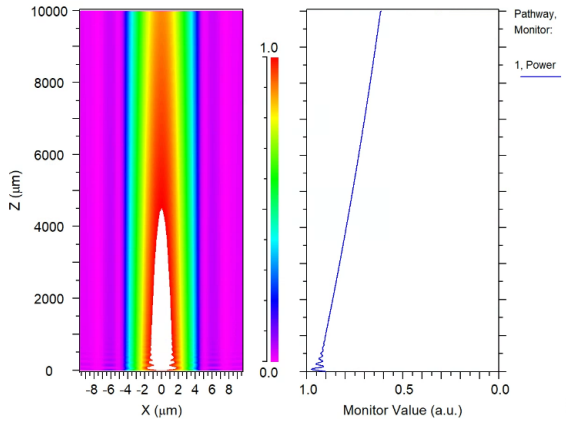


(b) Propagation of the fundamental mode for a structure composed of 2 rings with a pore configuration of 8/12

Figure 37: Propagation of the fundamental mode in single-ring and two-ring structures

Comparing Figures 37a, 37b, and 32a, we can observe that there is no significant increase in the number of oscillations during wave propagation. This finding suggests that adding a larger number of rings primarily enhances the efficiency of power transmission without necessarily promoting the generation of additional higher-order modes along the structure. Sin embargo, añadir más anillo también reduce la cantidad de pérdidas que presenta la onda durante su propagación, y por tanto esto resultaría que los modos superiores que se puedan formar se propaguen una mayor distancia sin sufrir grandes pérdidas. By carefully balancing the number of rings and the inter-pore spacing, we can optimize the structure's performance in terms of power transmission while still achieving the desired mode filtering capabilities.

### 7.2.6 Case with a high number of pores

As discussed in the previous sections, when the number of pores in the rings is increased, the inter-pore distance decreases, eventually approaching zero. This configuration transforms the structure into an optical fiber-like geometry, where the core consists of YAG crystal and the cladding is composed of a layer of air. In such a scenario, the propagation of an electromagnetic wave through the core follows the principles of optical fiber, relying on total internal reflections, rather than behaving as in a photonic crystal. Consequently, higher-order modes emerge during wave propagation. By drawing this analogy, it becomes possible to study the appearance of these modes by assuming that the V-parameter of this structure can be calculated in a similar manner to the V-parameter of an optical fiber [eq: 1], approximating $r$ as the distance from the core center to the pore surface.

By employing Equation 1, it is possible to calculate an initial approximation of the maximum radius that fulfills the condition for single-mode waveguiding in these structures at a wavelength of $\lambda = 1645$ nm:

$$r = \frac{\lambda \cdot V_{eff}}{2\pi \cdot \sqrt{n_{\text{core}}^2 - n_{\text{cladding}}^2}} = 0.4187876\mu\text{m} \tag{17}$$

This analysis indicates that the core diameter, $D_{\text{core}}$, must be smaller than $0.8375752\mu$m for the waveguide to support a single-mode, siendo this value is significantly smaller than the diameters of the structures we are simulating.

This initial approximation indicates that as the number of pores in the structure increases, it progressively resembles an optical fiber, enabling the emergence of higher-order modes beyond the fundamental mode, as discussed in Section 7.2.3.Additionally, our approximation also suggests that a larger core diameter further promotes the occurrence of higher-order modes in the structure, as mentioned in Section 7.2.4. A larger core diameter provides more space for the modes to propagate and interact, allowing for the formation of additional modes.

## 7.3 Results obtained from simulating the propagation of a wave transmitted from a single-mode fiber

Once the data obtained from the mode propagation simulations for each of the structures has been analyzed, the results obtained when simulating the propagation of a Gaussian wave with an MFD of 7.4 $\mu$m were examined following the same methodology as utilized in Sections 7.1 and 7.2. Furthermore, a comparison was made with the results obtained in the previous Section:

### 7.3.1 Normalized transmitted power as a function of the inter-pore spacing

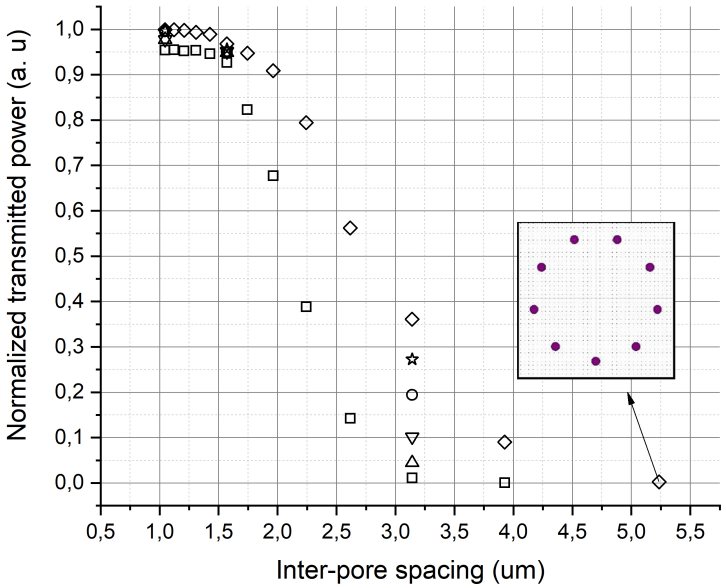


Figure 38: Single-ring structures

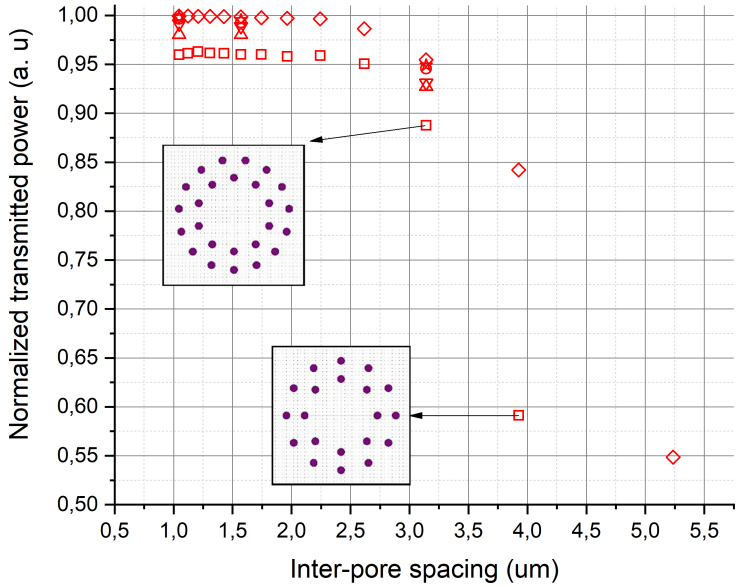


Figure 39: Two-ring structures

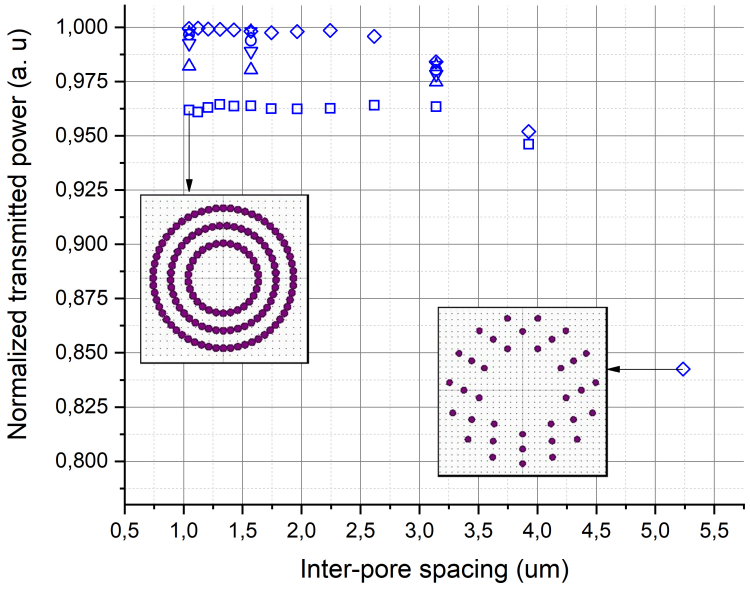


Figure 40: Three-ring structures

### 7.3.2 Normalized transmitted power as a function of the number of pores in the structure

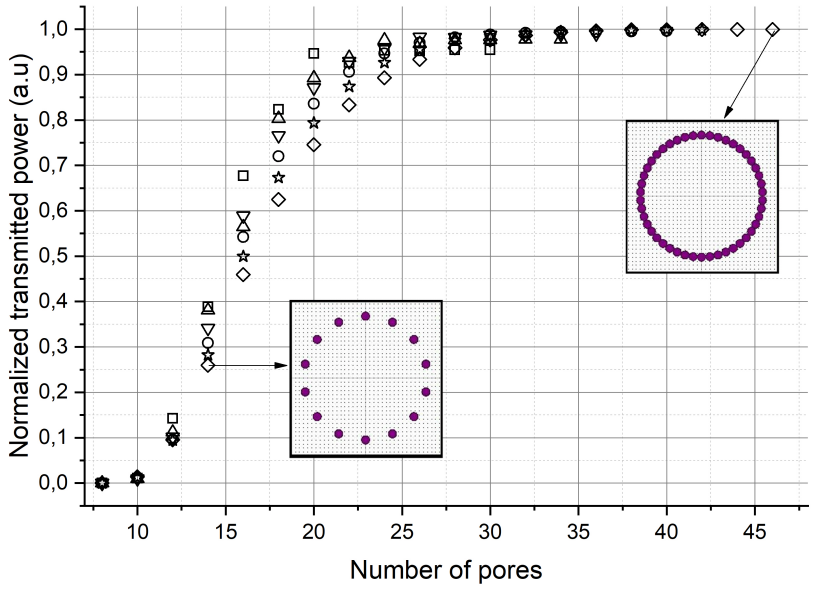


Figure 41: Single-ring structures

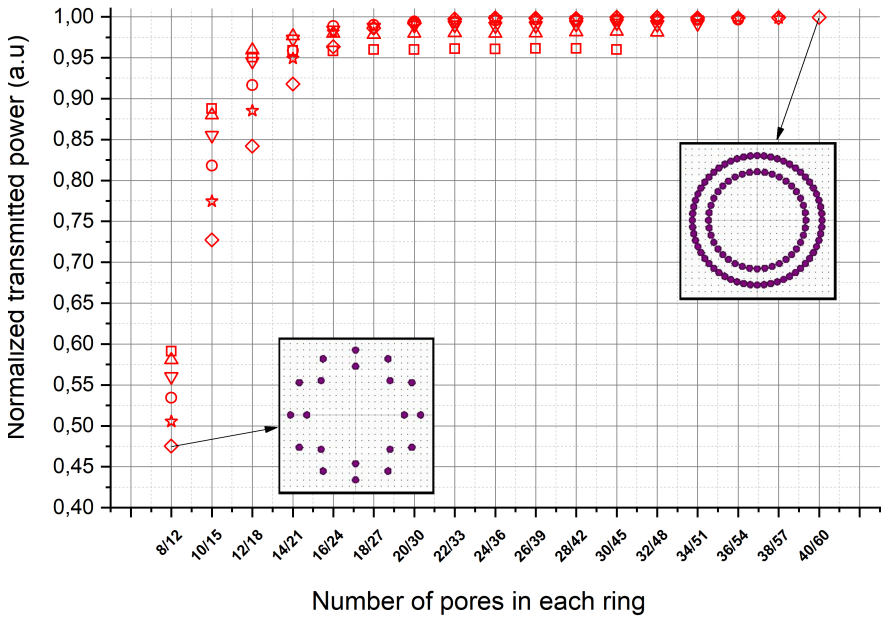


Figure 42: Two-ring structures

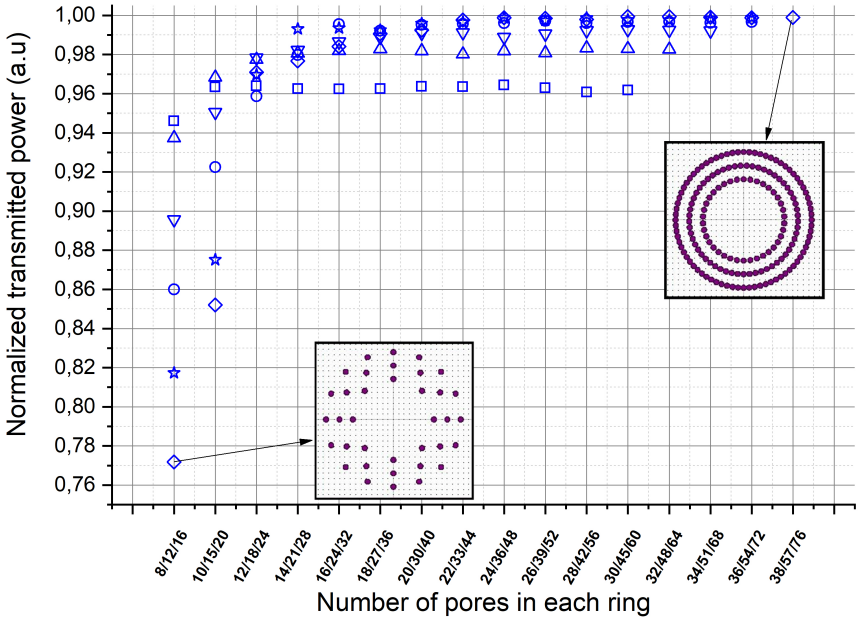


Figure 43: Three-ring structures

### 7.3.3 Losses in the coupling of these structures

As mentioned in the Methodology section, when connecting a single-mode fiber to a single-mode waveguide, losses occur in the coupling due to the difference in mode field diameter between the two guides. It is crucial to take these losses into account in such systems, and in our case, it is important to determine which types of structures exhibit higher losses of this nature. Therefore, using Equation 13, the relative power losses in the coupling of a fiber with MFD = 7.4 $\mu$m have been calculated for the range of D[1/e] values corresponding to the fundamental modes of the structures investigated in Section 6.5 (with the parameter D[1/e] being used as an equivalent parameter to the MFD of the fundamental mode in each structure):

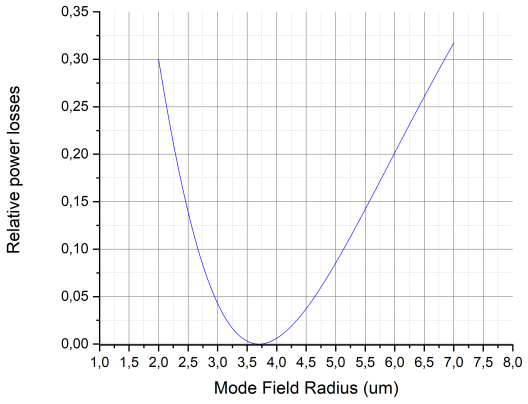


Figure 44: Power coupling losses as a function of mode field radius in the crystal structure

From the figure above, it can be observed that as the MFR (and thus the MFD) of the structure

increases relative to the MFR of the fiber, the losses are expected to increase as well. However, these losses are not reflected in the data obtained in Figures 38, 39, 40, 41, 42, 43. On the contrary, it is shown that with a larger core diameter and therefore a larger D[1/e] as discussed in Section 6.5, more power is transmitted. The anticipated losses should occur at the beginning of wave propagation through the structure; however, as demonstrated in the following example, this is not the case:

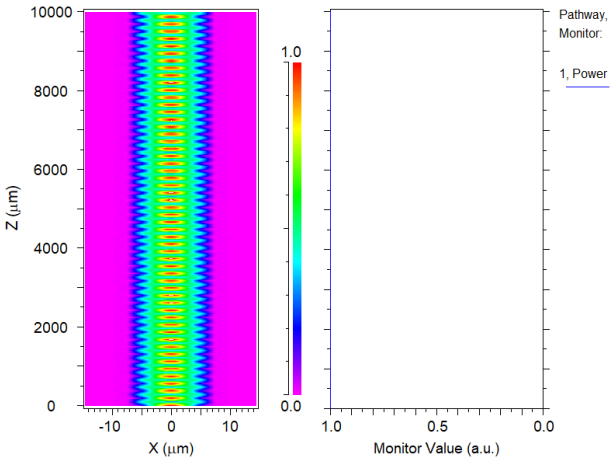


Figure 45: Propagation of a Gaussian wave with MFD=7.4 $\mu$m along a structure composed of 3 rings, with a core diameter of 15 $\mu$m and a pore configuration of 38/57/76.

The provided figure illustrates the propagation of a Gaussian wave in a 3-ring structure with a core diameter of D = 15 $\mu$m and a pore configuration of 38/57/76. Interestingly, the observed mode in this structure exhibits a D[1/e] value of 12.1308 $\mu$m (and therefore its MFR has a value of 6.0654 $\mu$m), which would typically suggest the occurrence of expected coupling losses. However, contrary to expectations, these losses are not observed. This phenomenon can be attributed to the fact that these structures allow the formation of higher-order modes in addition to the fundamental mode, indicating that they are not strictly single-mode structures.

Therefore, the differences in transmitted power observed in Figures 38, 39, 40, 41, 42, and 43 between structures with different diameters and a large number of pores or a low inter-pore spacing are due to the fact that a larger diameter allows a greater amount of wave energy to propagate through its core, while a smaller core diameter would propagate a lesser amount of this wave energy.

### 7.3.4 The Effect of Inter-Pore Spacing, Number of Pores in Each Ring, Core Diameter, and Number of Rings on Gaussian Wave Propagation

In Figures 38, 39, 40, 41, 42, and 43, we observe a similar behavior as described in the previous section. An increase in the number of pores in the rings (or equivalently a decrease in the inter-pore spacing) leads to an increase in the transmitted power, similar to the effect of increasing the number of rings in the structure as described in the previous section. To analyze these effects in greater detail, we will examine the propagation of a Gaussian wave through the structure using the following examples:

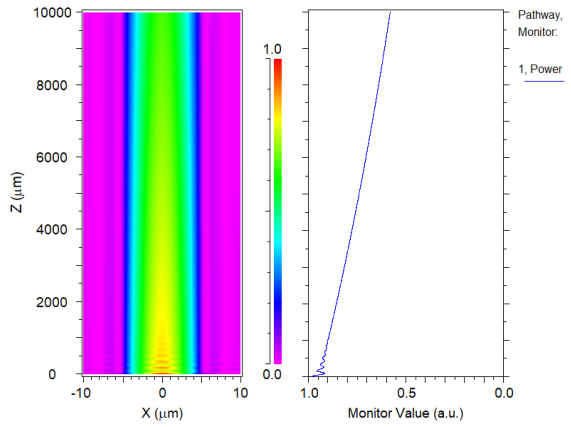


(a) Propagation of a Gaussian wave with MFD = 7.4 $\mu$m in a 2-ring structure with a core diameter of 11 $\mu$m and a pore configuration of 8/12

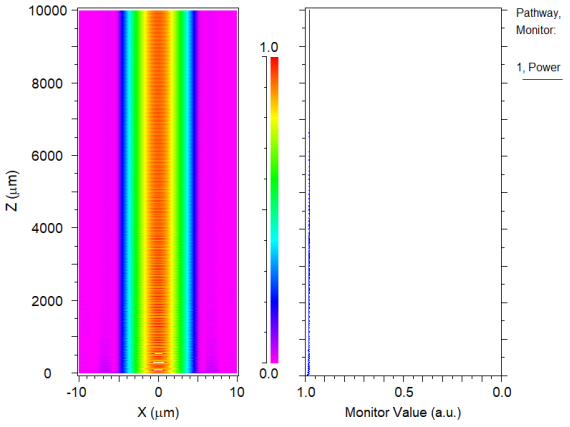


(b) Propagation of a Gaussian wave with MFD = 7.4 $\mu$m in a 2-ring structure with a core diameter of 11 $\mu$m and a pore configuration of 16/24

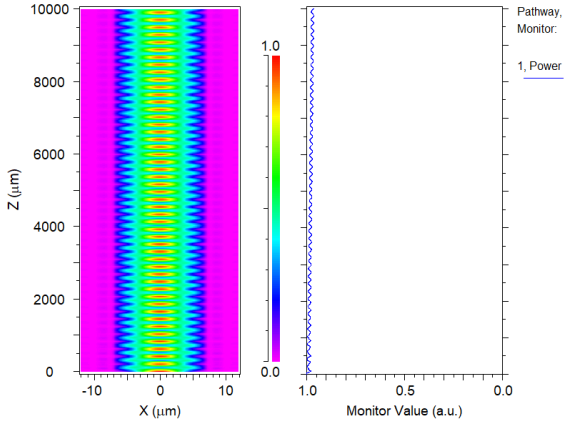


(c) Propagation of a Gaussian wave with MFD = 7.4 $\mu$m in a 2-ring structure with a core diameter of 15 $\mu$m and a pore configuration of 16/24

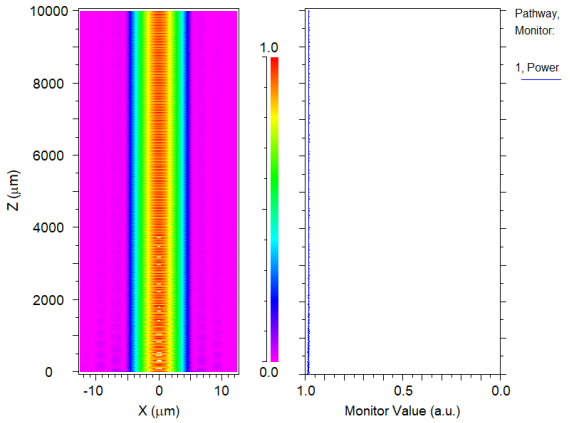


(d) Propagation of a Gaussian wave with MFD = 7.4 $\mu$m in a 3-ring structure with a core diameter of 11 $\mu$m and a pore configuration of 16/24/32

Figure 46: Propagation of Gaussian waves with MFD=7.4 $\mu$m in different structures

The previous figures demonstrate a consistent pattern that aligns with our previous observations: an increased number of pores in the rings, or a decreased inter-pore spacing, leads to a higher amount of transmitted power. Similarly, a higher number of pores corresponds to an increased power transmission.

We also observe a similar effect in the formation and propagation of higher-order modes within the structures. Increasing the number of pores promotes the formation and propagation of these modes, as does increasing the core diameter. On the other hand, adding more rings to the structure does not contribute to the formation of higher-order modes but does improve the amount of transmitted power. These phenomena align with the findings described in Section 7.2, validating the conclusions drawn in that section for this case as well.

### 7.3.5 Saturation Effect

In Figures 38, 39, 40, 41, 42, and 43, a saturation effect can be observed, where increasing the number of pores in the structure or reducing the inter-pore spacing does not significantly improve

the transmitted power. This saturation effect is particularly advantageous considering the high precision and substantial time required for fabricating pores in a photonic crystal. Consequently, this saturation effect allows the creation of structures with fewer pores while maintaining effective light propagation.

To study this effect, each plot will be divided into two distinct regions. The first region will include structures whose transmitted power is greater than 95% of the maximum power transmitted for structures with a core diameter of 10 $\mu$m:

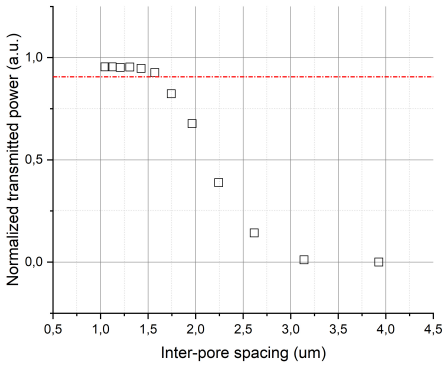


(a) Single-ring structures with a core diameter of 10 micrometers

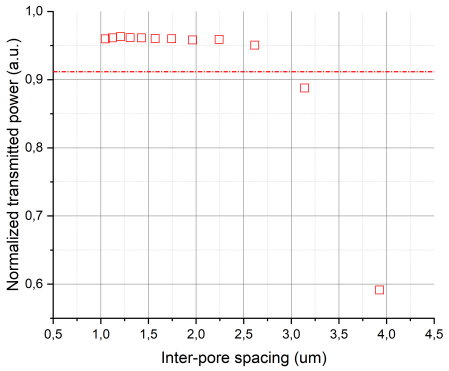


(b) Two-ring structures with a core diameter of 10 micrometers

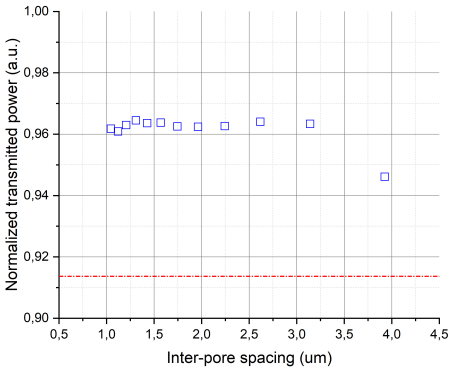


(c) Three-ring structures with a core diameter of 10 micrometers

Figure 47: Normalized transmitted power for different structures with varying number of rings and a core diameter of 10 micrometers

Based on the figures presented, it is clear that there exists a threshold value for the inter-pore spacing. Below this threshold, decreasing the inter-pore spacing has a noticeable impact on the transmitted power of the structure. However, once the threshold is surpassed, further reduction in the inter-pore spacing has limited effect on the transmitted power. This threshold value varies depending on the specific characteristics of the structure. Additionally, it is worth noting that an increase in the number of rings within the structures leads to a higher proportion of structures surpassing the established threshold. This observation highlights the influence of the number of rings on the saturation effect

This saturation effect is so interesting because it could help us to solve the main problems when elaborating this type of structures, allowing us to create structures with an inter-pore spacing value that avoids the appearance of defects in the crystal, while preserving the ability to eliminate the non-fundamental modes characteristic of these structures without suffering a significant amount of losses during the wave propagation.

# 8 Conclusion

En esta sección se presentan las conclusiones derivadas del análisis de las estructuras de cristal fotónico. Se observó que aumentar el número de poros o reducir el espaciado entre ellos confina el modo fundamental dentro del núcleo y produce una distribución de campo más simétrica. El tamaño del núcleo mostró una relación positiva con el parámetro D[1/e], lo que indica que un mayor diámetro del núcleo resulta en un valor más alto de dicho parámetro. Sin embargo, agregar más anillos a la estructura no afecta significativamente la distribución del modo fundamental. En cuanto a la potencia transmitida, se encontró una relación positiva entre el número de poros (o la disminución del espaciado entre ellos) y la potencia transmitida por la onda, a costa de aumentar la formación y propagación de modos superiores al modo fundamental. Si se mantiene constante el espaciado entre poros, aumentar el diámetro del núcleo permite una mayor potencia transmitida. Sin embargo, si se mantiene constante el número de poros, un mayor diámetro del núcleo resulta en mayores pérdidas de potencia y un aumento en la formación de modos superiores al modo fundamental. Además, se halló que aumentar el número de anillos incrementa la potencia transmitida sin aumentar la formación de modos superiores al modo fundamental. En las simulaciones de propagación de una onda Gaussiana de MFD=7.4 $\mu$m, no se observaron las pérdidas de acoplamiento esperadas al conectar dos guías de onda monomodo, lo que indica que las estructuras de cristal fotónico permiten la formación de modos superiores al modo fundamental. También se observó un efecto de saturación, donde un aumento adicional en el número de poros tiene un impacto insignificante en la potencia transmitida. Basándonos en los resultados obtenidos, se considera como áreas de interés para investigaciones futuras el análisis detallado de las estructuras compuestas por dos y tres anillos, con configuraciones de poros de 8/12 y 8/12/16 respectivamente, y un diámetro de núcleo de 10 $\mu$m. En cuanto a futuras líneas de trabajo, sería interesante considerar las pérdidas de absorción y de difracción en las simulaciones, así como realizar pruebas empíricas para relacionar y verificar los resultados obtenidos. Esto permitiría obtener un mayor conocimiento sobre las estructuras de cristal fotónico y su comportamiento en condiciones reales.

In conclusion, the analysis of photonic crystal structures provides valuable insights into optimizing their performance by understanding the relationships between various parameters. The first part of the results reveals that increasing the inter-pore spacing widens the mode field distribution, indicating a wider spread of the wave within the structure. On the other hand, denser structures with smaller inter-pore spacing confine the wave closer to the core, resulting in a narrower and more symmetrical mode field distribution.

A linear relationship is observed between D[1/e] and the core diameter, indicating that a larger core diameter allows for more energy to be carried by the wave within the structure, resulting in a wider distribution of the fundamental mode field.

In contrast, the number of rings in the structure has minimal impact on the mode field distribution, as it is primarily determined by the first ring of pores. Additional rings contribute to wave propagation and stability but have minimal influence on the fundamental mode field distribution.

In the second part, upon analyzing the propagation of the fundamental modes in their corresponding structures, it is inferred that increasing the number of pores (or equivalently decreasing the inter-pore spacing) also increases the power transmitted by the structure. However, this simultaneous increment also results in the generation and propagation of higher-order modes alongside the fundamental mode.

In relation to the core diameter, it is observed that increasing the core diameter while maintaining a constant inter-pore spacing enables better concentration of wave energy within the core, leading to higher transmitted power. However, if the number of pores remains constant, further increase in the core diameter can result in increased energy loss and reduced transmitted power due to a larger inter-pore spacing. Nevertheless, once a sufficiently high number of pores is reached, the variation in diameter does not significantly impact the transmitted power. Additionally, it is noted that a larger core diameter facilitates the formation of a greater number of higher-order modes during propagation.

Adding more rings to the structure significantly increases the power transmission without a significant increase in the formation of higher-order modes. However, these higher-order modes would also experience fewer losses during propagation. The interplay between inter-pore spacing, core diameter, and the number of rings influences this saturation effect, with a threshold value for inter-pore spacing determining its impact on the transmitted power.

As the number of pores increases and the inter-pore distance approaches zero, the structure exhibits characteristics similar to an optical fiber, with the emergence of higher-order modes during wave propagation. This approach concluded that larger core diameters and more pores promote the occurrence of higher-order modes, providing more space for their propagation and interaction.

In the final part of the analysis, it is observed that photonic crystal structures exhibit coupling losses and power transmission that deviate from traditional expectations based on mode field diameter, highlighting their multimode behavior.

Furthermore, a saturation effect has been observed in the results, indicating that this is a useful tool for fabricating structures that enable efficient power transmission while maintaining the ability to filter higher-order modes.

Based on these findings, it is possible to determine the parameters necessary for achieving efficient wave propagation through a photonic crystal structure while simultaneously suppressing higher-order modes. As a result, two intriguing structures to investigate further are those with a 10 $\mu$m core diameter and pore configurations of 8/12 and 8/12/16. Despite the notable differences in transmitted power between the two-ring structure with the 8/12 pore configuration and the three-ring structure with the 8/12/16 pore configuration, the former demonstrates its effectiveness in mitigating higher-order modes. Moreover, the similarities between these two structures facilitate a more straightforward comparative analysis of their respective results.

For future lines of research, it would be interesting to conduct simulations taking into account the absorption capability of the crystalline material and the losses due to diffraction that the propagating wave could experience. It would also be valuable to explore further configurations of these

structures, such as smaller core diameters, to assess potential coupling losses and their impact on the formation of higher-order modes within the crystal. Additionally, it would be advisable to validate the obtained simulation results through empirical testing and verify if these results align with those obtained from the simulations. In case of any discrepancies, it is important to identify and understand the reasons behind them. This will contribute to a comprehensive understanding of the behavior and performance of photonic crystal structures.

## References


[1] Norman P. Barnes, Brian M. Walsh, Farzin Amzajerdian,Donald J. Reichle, George E. Busch, and William A. Carrion *Up conversion measurements in Er:YAG; comparison with 1.6 $\mu m$ laser performance*

[2] Coherent Inc. (2021). Specialty Optical Fibers: Single-Mode Graded-Index (SM-GDF-6/125-M). Access Date: July 7, 2023. URL: `https://coherentinc.my.site.com/Coherent/specialty-optical-fibers/SM-GDF-6_125-M?cclcl=en_US`

[3] M. O. Iskandarov and A. A. Nikitichev *Quasi-two-level $Er^{+3}$:$Y_3Al_5O_{12}$ laser for the 1.6-mm range*

[4] J. W. Kim, D. Y. Shen, J. K. Sahu, and W. A. Clarkson, *High-power in-band pumped Er:YAG laser at 1617 nm*

[5] Thorlabs. "The Mode Field Diameter". Access Date: July 7, 2023. URL: `https://www.thorlabs.com/newgrouppage9.cfm?objectgroup_id=14203`

[6] RP Photonics Consulting GmbH. "Mode Radius". Access Date: July 6, 2023. URL: `https://www.rp-photonics.com/mode_radius.html`

[7] RP Photonics Consulting GmbH. "V Number". Access Date: July 6, 2023. URL: `https://www.rp-photonics.com/v_number.html`.

[8] Joannopoulos, J. D., Johnson, S. G., Winn, J. N., Meade, R. D. (2008). Photonic Crystals: Molding the Flow of Light, 2nd Edition. Princeton University Press

[9] Paz-Buclatin, F., Esquivel-González, M., Casasnovas-Melián, A., de Varona, O., Cairós, C., Trujillo-Sevilla, J. M., Kamada, K., Yoshikawa, A., Rodríguez-Ramos, J. M., Martin, L. L., & Ródenas, A. (2022). *Circularly symmetric nanopores in 3D femtosecond laser nanolithography with burst control and the role of energy dose. Nanophotonics.* Advance online publication: `https://doi.org/10.1515/nanoph-2022-0665`

[10] Ródenas Seguí, A. (Capítulo 20). Subtractive 3D Laser Nanolithography of Crystals by Giant Wet-Chemical Etching Selectivity

[11] Osellame, R., Cerullo, G., & Ramponi, R. (Eds.). (2012). *Femtosecond Laser Micromachining: Photonic and Microfluidic Devices in Transparent Materials.* Springer.

[12] Synopsys. "CAD Environment for Photonic Device Tools". Access Date: July 6, 2023. URL: `https://www.synopsys.com/photonic-solutions/rsoft-photonic-device-tools/cad-environment.html`

[13] Synopsys, Inc. (2021). *Photonic Solutions BeamPROP BPM v2021.09 User Guide.*

[14] Synopsys, Inc. (2022). *Photonic Solutions WinPLOT v2022.09-1 User Guide.*

# Appendix

## A Explanation of how the simulations were conducted

In this study, we focus on an optical system that comprises an Er:YAG crystal with a concentric ring structure formed by pores. This system receives a Gaussian wave with a wavelength of 1645 nm from a conventional optical fiber. To this part, we adopt the specifications of the "6/125 Precision Matched Passive Single-Mode 1550-nm Double Clad Fiber", which has a mode field diameter (MFD) of 7.4 $\mu$m. We have selected this fiber due to its cost-effectiveness and widespread usage in the field.

Our objective was to simulate the propagation of a linearly polarized Gaussian wave with a mode field diameter (MFD) of 7.4 $\mu$m along a Er:YAG crystal of length 10 mm, considering various configurations of the concentric pore ring structure. We aimed to determine the transmitted power of the wave as it passes through the crystal.

In the *RSoft CAD: BeamProp* program, the creation of photonic crystal structures, including our specific case of pore structures in concentric rings, is made straightforward.

As an example, the image below showcases a 3 concentric ring pore structure. The pores are visualized as purple cylinders, while the white background corresponds to the remaining Er:YAG crystal.

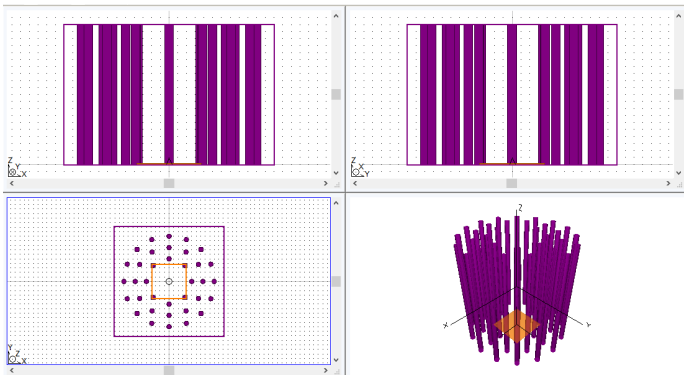

Figure 48: Example of a 3 concentric pore ring structure in BeamPROP

To configure the structure accurately, the program provides multiple control panels where users can define the parameters for simulation. In this section, we will introduce each control panel and explain its functionality, beginning with the *Global Settings Window* control panel:

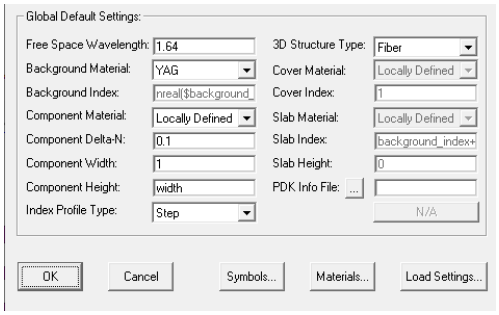


Figure 49: Control Panel *Global Settings Window* in BeamPROP

In the *Global Settings Window* control panel, essential parameters for the simulation are defined, including the wavelength of the simulated wave, the refractive index of the background, and the type of background material.

For our specific simulations, we have configured the following options in the control panel:

- *Free Space Wavelength*: We have set a wavelength of 1645 nm for the simulations.
- *Background Index*: The refractive index of the YAG material, which serves as the background for the simulation, was entered as $n = 1.8057$.
- *Delta-N Component*: This option requires specifying the refractive index difference between the crystal and the pores. Since we want the pores to have the refractive index of air, we assign the value $n_{\text{air}} - n_{\text{YAG}} = -0.8057$.
- *3D Structure Type*: We choose the "Fiber" option to shape the air pores as cylindrical structures.
- *Component Width*: The standard width of the simulated pores is set to 1 $\mu$m.
- *Component Height*: A standard height of 1 $\mu$m is established for the pores to ensure their circular shape.

It is worth noting that there are additional customization options available in this control panel, but for our study, they are not relevant and will not be explained in detail.

To create cylinders representing the pores of the photonic crystal in the *RSoft:CAD* program, the *Segment* option is selected from the toolbar on the left-hand side of the program interface [fig:4]. By left-clicking on the white background and dragging, a segment is formed. Right-clicking on the segment opens a control panel where parameters can be adjusted. This panel allows for modification of properties such as length, width, height, position, and orientation of the segment, enabling customization of the cylinder to match the desired dimensions and spatial arrangement within the photonic crystal structure.

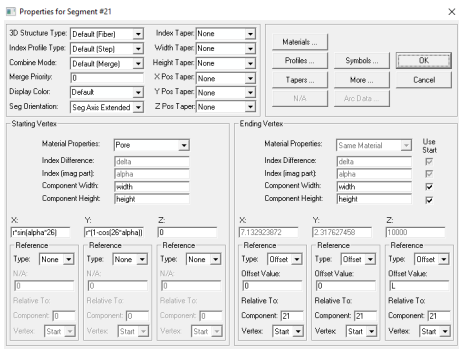


Figure 50: Properties dialog box of the segment

In this panel, modifications can be made to the shape, width, height and refractive index of the selected segment, if different values from those set in the *Global Settings Window* panel are desired. In addition, it is possible to set the specific position of the segment.

To set the segment position, two panes are used. In the lower left panel, the coordinates of the centre point of one of the cylinder faces that will form the pore are defined. In the lower right-hand panel of coordinates, the length of the pore is set, which in our case is specified to have a length of 10 mm, indicating this value in the *Offset Value* section of the Z-coordinate in the lower right-hand panel. The other *Offset Value* for the X and Y coordinates are kept at 0, as we only want the pore to be parallel to the Z axis.

To complete the configuration, we need to define the properties of the wave we want to simulate. The wavelength has already been specified, but we also need to define the initial position and width of the wave, as well as its distribution type. This can be done in the following control panel:

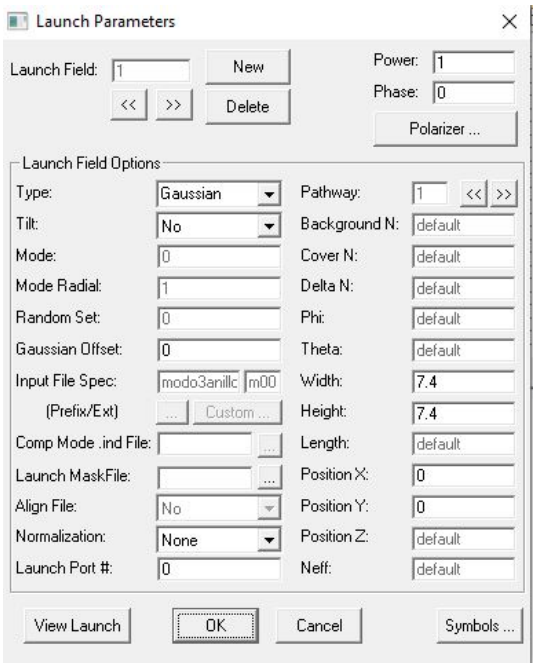


Figure 51: Dialog box for the Launch Parameters

In the *Wave Settings Window* control panel, we can configure the parameters for the wave simulation. Specifically, we will focus on the settings used in the simulations, omitting other options that were not utilized:

- *Type*: This option allows for the selection of the wave distribution to be simulated, such as a Gaussian distribution, which was the option used in the simulations. The *File* option was also utilized, which enables loading a file with customized data for the wave distribution to be simulated. This option was used to select the files obtained from the field distribution of the modes and simulate their propagation.
- *X-position* and *Y-position*: These parameters specify the coordinates of the wave's launch center. In our simulations, the origin point (0,0) was chosen.
- *Width* and *Height*: These parameters define the dimensions of the wave launch area. In Figure 48, this area is represented as an orange rectangle.

If a Gaussian distribution is chosen, the input field is described by the following function:

$$f(x,y) = e^{(\frac{-x^2}{a^2})} \cdot e^{(\frac{-y^2}{b^2})} \tag{18}$$

a = w/2 and b = h/2, and w and h are the previously selected *Width* and *Height*. Therefore, to simulate a wave with MFD=7.4 $\mu$m, the *Width* and *Height* options were configured to have a value of 7.4 each.

It is also possible to define and modify the polarization of the simulated wave. In our case, for the sake of simplicity, we have opted for the default configuration, which corresponds to linear polarization along the $E_x$ axis.

The *BeamPROP* software is employed to calculate the steady-state optical field throughout an entire design file. It is commonly useful to analyze this field in standard physical quantities, such as the optical power in a specific region of the circuit or the power traveling in a particular mode.

To enable such measurements, pathway monitors are utilized. Results are output as a function of the propagation direction Z and are measured along a pathway. For this purpose, a cylinder-shaped figure is created and placed inside and along our concentric ring structure, specifically within the core. This cylinder is configured with an *Inactive Index Profile Type* (configuration option shown in Figure 50), ensuring that its presence does not affect the simulations conducted. Once this cylinder is defined, we select the *Edit Pathway* option from the left-side toolbar of the program and choose this new cylinder as a new *Pathway*.

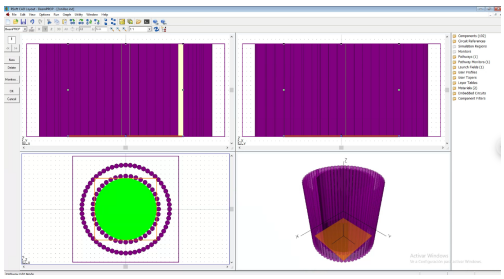

Figure 52: Selection of the New Cylinder as *Pathway*

After defining the new *Pathway*, we select the *Edit Pathway Monitors* option, also located in the left-side toolbar. This opens a dialog box in which we can specify the conditions for measuring the wave power while it propagates through the structure. Among the various configuration options presented, only two are of interest for our simulations: the *Monitor Type option* and the *Monitor Normalization Option*:

- *Monitor Type option*: This option controls the type of data measured and saved by a pathway monitor. In our case, we use the *Partial Power* configuration, which allows us to measure the power of the wave within the region of our core.
- *Monitor Normalization Option*: This option determines how the output of the pathway monitor is normalized. The default choice is *Input Power*, which normalizes power pathway monitors to the total power in the launch field. This option is used in our simulations.

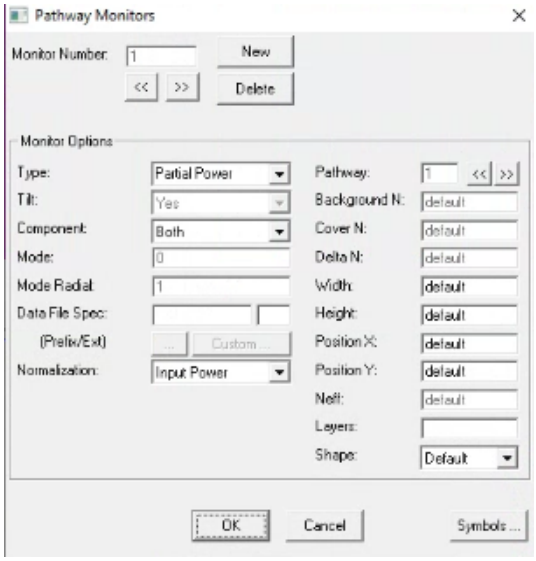


Figure 53: Pathway Monitor dialog box

In order to conduct the simulations, the *BPM Simulation Parameters* dialog box is utilized. *BeamPROP* solves the electromagnetic fields within a structure in a computational domain using a spatial mesh. Accurate results depend on correctly defining this mesh. Numerical parameters are specified in each spatial direction within the *BPM Simulation Parameters* dialog box.

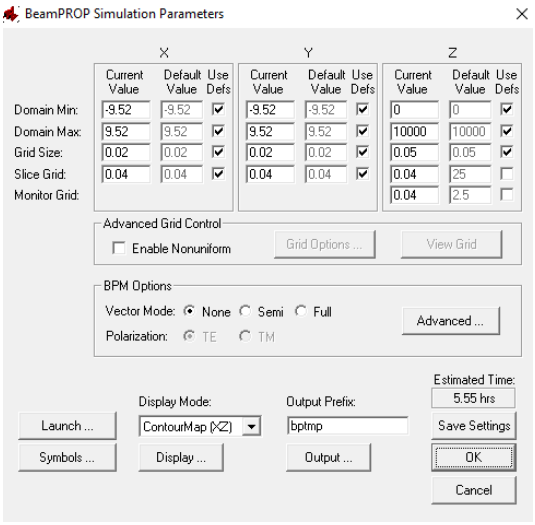


In the previous figure, the configuration of spatial mesh information is depicted:

- *Domain Minimum* and *Domain Maximum*: These settings define the boundaries of the simulation domain, i.e., the spatial range within which the simulation will take place. In our simulations, we used the default value automatically set by the program.
- *Grid Size*: Refers to the size of the mesh used to discretize the simulation space. This option affects the resolution and accuracy of the simulation. A smaller grid size enhances resolution by allowing more points in the mesh, but it also increases computational requirements. In our case, we used the default value.
- *Slice Grid*: Refers to the discretization in the direction of wave propagation. This option divides the propagation direction into sections or slices. A finer slice grid enables capturing fine details in wave propagation but may require more computational resources. Similarly, we used the default value in this case as well.

In the *Output Prefix* setting, you specify the name under which you want to save the output data of the simulation. Once everything has been configured, click on the *Ok* button to start the simulation.

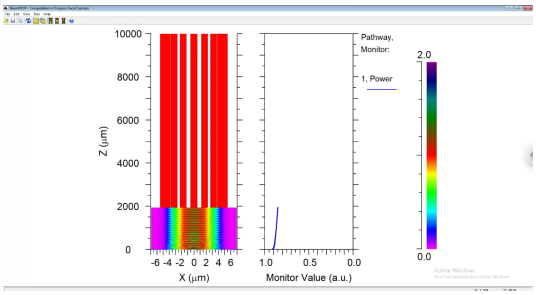


Figure 54: Simulation of wave propagation with the parameters described above in a structure consisting of a single ring with 18 equispaced pores.

In the previous figure, the left side illustrates the program's simulation of wave propagation along the structure, while the right side indicates the value of the wave power along the structure.

Finally, it would be necessary to mention the control panel *Symbols*:

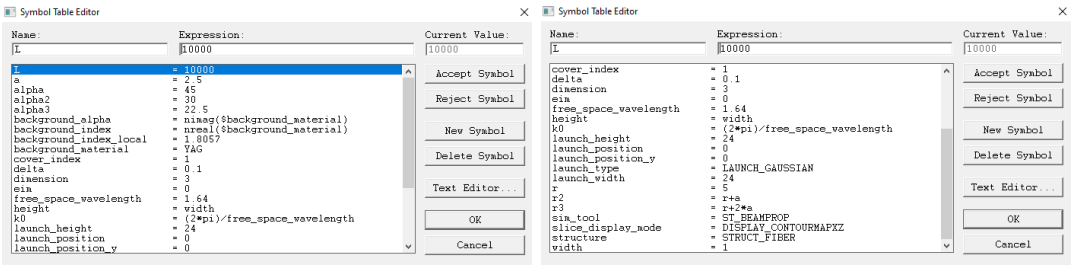


Figure 55: Control panel *Symbols* in BeamPROP

In this control panel, several important parameters are defined to configure the simulation accurately. These include the pore spacing distance, the diameter of each simulated ring, and other relevant constants.

## A.1 How the fundamental modes of each structure were obtained

In this work we analyze the electric field distribution of the fundamental modes of the waves generated by the Er:YAG crystal.

To find the modes of each structure, we utilize the panel *Mode Calculation Parameters*, which is used to calculate the different modes of the structure. Similar to the previous case, a domain needs to be defined in this panel as well:

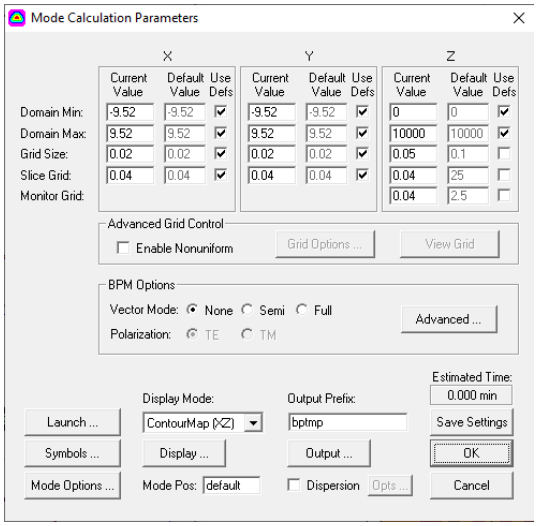


Figure 56: Mode Calculation Parameters dialog box

Unlike the previous case, where we used the default values of the program to simulate this domain, in this case, the values of the *Grid Size* and *Slice Grid* were set to 0.001 and 0.002, respectively. This ensured that the program was able to find the modes of the structures.

The program calculates the modes of the structure by simulating wave propagation and varying its parameters until the mode belonging to the simulated structure is found. The wave used by

the program to calculate the different modes of a structure is defined in the dialog box shown in Figure 51. It is recommended to use a Gaussian distribution for the wave and leave the properties at their default values. Therefore, this was the configuration used to calculate the modes.

In our case, we are only interested in the fundamental modes. Therefore, to instruct the program to calculate only the fundamental modes, we select the *Mode Options* from the dialog box shown in Figure 56, which opens a new window:

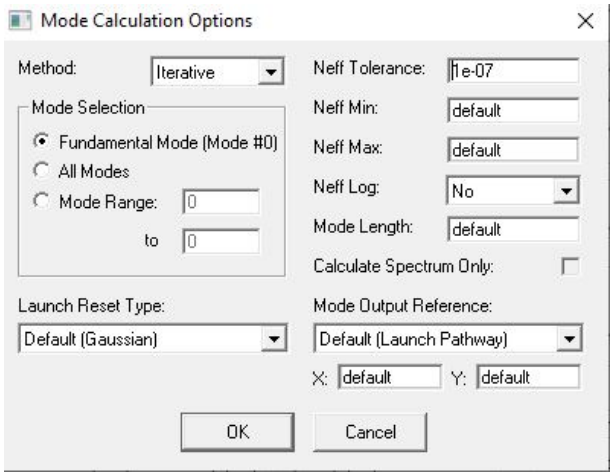


Figure 57: Picture of how the program calculates the modes of a structure.

In this new window, we select the *Fundamental Mode (Mode #0)* option to instruct the program to calculate only the fundamental mode of the structure.

After configuring all the settings, we initiate the simulation by clicking the *OK* button, as depicted in Figure 56.

Upon completion of the simulation, the data is saved in the designated folder specified in the *Output Prefix* option.